

Select, then Balance: A Plug-and-Play Framework for Exogenous-Aware Spatio-Temporal Forecasting

Wei Chen¹, Yuqian Wu¹, Yuanshao Zhu^{2,3}, Xixuan Hao¹, Shiyu Wang⁴, Yuxuan Liang^{1†}

¹Hong Kong University of Science and Technology (Guangzhou)

²Southern University of Science and Technology, ³City University of Hong Kong, ⁴ByteDance
onedeansxx@gmail.com, ywu188@connect.hkust-gz.edu.cn, yuxliang@outlook.com

ABSTRACT

Spatio-temporal forecasting aims to predict the future state of dynamic systems and plays an important role in multiple fields. However, existing solutions only focus on modeling using a limited number of observed target variables. In real-world scenarios, exogenous variables can be integrated into the model as additional input features and associated with the target signal to promote forecast accuracy. Although promising, this still encounters two challenges: the inconsistent effects of different exogenous variables to the target system, and the imbalance effects between historical variables and future variables. To address these challenges, this paper introduces **ExoST**, a novel framework for modeling exogenous variables in spatio-temporal forecasting, which follows a “select, then balance” paradigm. Specifically, we first construct a latent space gated expert module, where fused exogenous information is projected into a latent space to dynamically select and recompose salient signals via specialized sub-experts. Furthermore, we design a siamese network architecture in which recomposed representations of past and future exogenous variables are fed into dual-branch spatio-temporal backbones to capture dynamic patterns. The outputs are integrated through a context-aware weighting mechanism to achieve dynamic balance during the modeling process. Extensive experiments on real-world datasets demonstrate the effectiveness, generality, robustness, and efficiency of our proposed framework.

1 INTRODUCTION

Spatio-temporal forecasting aims to model the dynamic evolution of spatial entities over time by leveraging historical spatio-temporal sequences to predict future states over multiple time steps [12, 13, 17, 45]. This task finds critical applications in domains such as traffic management [4, 57], environmental monitoring [32, 52], and weather forecasting [7, 59]. In recent years, researchers have developed various spatio-temporal (ST) neural encoders [25, 26] by combining building blocks with different relational inductive biases, such as graph convolution operator [30, 38, 60] for spatial dependencies and sequence operator [21, 56] for temporal patterns. However, these approaches predominantly rely on modeling limited observations of target system variables, focusing mainly on encoding the spatial and temporal dynamics of target signals, while overlooking a widely available yet underutilized source of information in real-world forecasting systems: spatio-temporal exogenous variables.

Spatio-temporal exogenous variables refer to contextual information that is related to the prediction system but originates from external dynamic systems [6]. Such variables may include historical information that co-occur with the target system as well as prior information about future time points provided by external

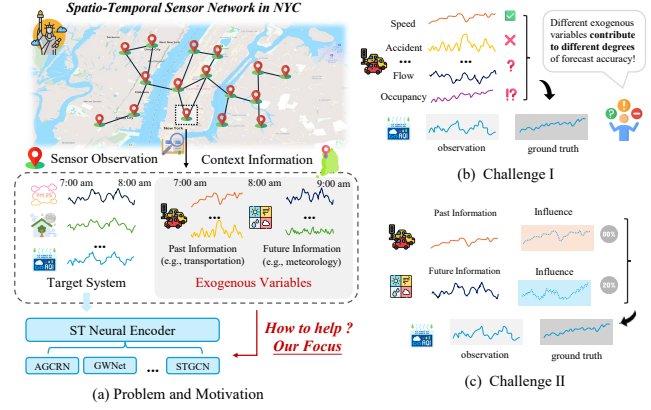


Figure 1: Problem and motivation statement.

auxiliary forecasting systems. These factors serve as critical complementary signals in prediction tasks, helping to reduce uncertainty while offering interpretability [3, 14, 20, 22, 40, 53]. As illustrated in Fig. 1 (a), consider the sensor network of air quality monitoring stations in New York City. For any given monitoring station, air quality forecasting typically focuses on modeling various indicators of pollutant emissions (e.g., NO_2 , CO_2) to predict future air conditions. However, air quality at a particular location may also be significantly influenced by surrounding contextual information. For instance, historical traffic congestion data in the region (e.g., traffic flow) could lead to sudden spikes in pollutant levels, while stable weather conditions predicted for the future (e.g., wind speed) may indicate a risk of continued deterioration in air quality.

Despite the considerable potential of incorporating exogenous information, two major challenges persist in practice:

◆ **Challenge I: Inconsistent Variable Effects:** In real-world scenarios, exogenous variables often exert varying degrees of influence on the prediction target. As shown in Figure 1(b), different exogenous variables display distinct temporal dynamics and correlations with the target signal. Some variables (e.g., traffic flow) may have substantial predictive value, while others (e.g., traffic incidents) may be marginally relevant or even introduce noise. Fig. 2 (a) further illustrates this phenomenon by showing the Pearson correlation coefficients between various exogenous variables and the target variable across randomly selected stations in the *AQI-19* dataset. Despite this variability, existing approaches often adopt a one-size-fits-all strategy [3, 20], directly concatenating exogenous variables with input features, without selectively modeling their individual contributions. This lack of mechanism-aware integration limits performance and can even degrade predictive accuracy.

◆ **Challenge II: Imbalanced Type Effects:** In addition to inter-variable disparities, there also exist imbalanced type differences

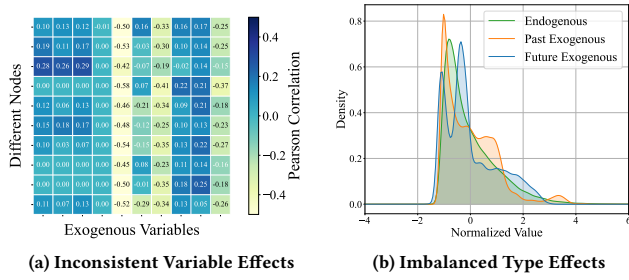


Figure 2: A case study of inconsistent variable effects and imbalanced type effects in the AQI-19 dataset.

between past and future exogenous variables from different temporal contexts. As shown in Fig. 1(c), exogenous information may stem from historically perceived signals (e.g., past traffic data) or from proactively forecasted future signals (e.g., weather predictions), leading to temporal distribution asymmetry and context-dependent impacts on prediction outcomes. Fig. 2 (b) clearly demonstrates the distinct distribution patterns of normalized values across different types of exogenous variables in the AQI-19 dataset. Existing methods typically adopt joint modeling strategies that fail to distinguish the distinct influences of these two types of exogenous variables on the target system [14, 40, 53, 62]. Moreover, even under decoupled modeling settings, simple weighted fusion is insufficient to effectively balance their heterogeneous effects.

To address the aforementioned challenges, we propose a novel exogenous variable-enhanced spatio-temporal forecasting framework, **ExoST**, which is built upon a core “select, then balance” paradigm to systematically exploit and integrate the contributions of exogenous variables, thereby improving overall predictive performance. The framework adopts a modular and flexible design that allows seamless integration with a wide range of mainstream spatio-temporal backbone networks. Specifically, ❶ we introduce an adaptive selection mechanism through a latent-space gated expert module, which projects both endogenous and multi-source exogenous variables into a condition latent space and activates specialized expert sub-networks via a gating mechanism. This enables the model to automatically select and combine the most informative exogenous factors. The module exhibits strong representational capacity and adaptability, effectively capturing relevant signals while suppressing irrelevant or redundant information, thus alleviating inconsistencies caused by variable heterogeneity. To address the imbalance between types of exogenous variables, ❷ we design a dual-branch siamese network architecture that independently models past and future exogenous information. These recomposed representations are fed into dual versions of any given spatio-temporal backbone to learn evolutionary patterns, and a context-aware balancer is employed to dynamic fusion and produce the final prediction.

In summary, our key contributions are as follows:

- **Adaptive Selection Mechanism for Inconsistent Variable Effects:** We propose a Latent Space Gated Expert Module that effectively handle the latent associations among multi-source exogenous variables. Through an expert selection mechanism, it identifies and emphasizes the most predictive external signals, enhancing the quality of the semantic representation input.

- **Balance Modeling Strategy for Imbalanced Type Effects:** We design a Siamese network architecture that separately models past and future exogenous information branch, enabling dynamic prediction balancing via a context-aware fusion gating mechanism.
- **A Flexible Plug-and-Play Framework:** **ExoST** provides a general and flexible enhancement framework for spatio-temporal forecasting. It can be broadly applied to various backbones and consistently outperforms existing methods across multiple benchmarks, demonstrating both practical value and scalability.

2 PRELIMINARIES

2.1 Related Work

2.1.1 Spatio-Temporal Forecasting. Predicting future spatio-temporal signals from historical observations, a spatially extension of multivariate time series forecasting, has evolved significantly. Early statistical [8, 9] or independent time series models [16, 39, 42, 44, 55] at each location proved insufficient for complex spatio-temporal dynamics [46], which involve intricate spatial correlations and heterogeneity [12, 13]. This led to hybrid architectures [10, 21, 29, 30, 37, 38, 47, 56] that integrate spatial (e.g., graph operators for node interactions) and temporal (e.g., sequence operators for long-term trends) modeling to jointly learn rich spatio-temporal representations for accurate prediction. *However, a critical limitation persists: these models largely focus on the system’s internal dynamics while neglecting exogenous variables—external inputs that are independent of the system’s state but directly influence its evolution, and whose inclusion is vital for robust and accurate predictions.*

2.1.2 Exogenous Variables Modeling. In practical time series forecasting scenarios, exogenous information is already integrated into the model as additional input features and concatenated with the target signal, enabling the model to learn the correlation between external factors and the target variable. Earlier studies explored statistical methods such as ARIMAX [54] and SARIMAX [51] that can understand the relationship between exogenous and endogenous sequences and autoregression. Advanced deep learning models discuss how to use future values of exogenous variables [14, 40] and how to adapt to time lags and missing exogenous variable data scenarios [53, 62]. In addition, some works [22, 28, 36] also discuss how to use language models to align the semantic information of exogenous variables for enhancement. Limited works have explored the integration of exogenous variables in spatio-temporal forecasting scenarios, but they only focus on specific task scenarios and model structure design [15, 20, 33, 61]. *In contrast, we systematically explore how to effectively model exogenous variables in spatio-temporal forecasting scenarios and adaptively weigh the impact of different exogenous variables.*

2.2 Problem Formulation

DEFINITION 1. (Spatio-Temporal Data). Spatio-temporal data refers to observational records that capture how dynamic systems evolve in space and time. Each data point is associated with a specific geographic location and a specific timestamp. This type of data can usually be represented as a temporal sequence $X = \{X_t\}_{t=1}^T$, where each $X_t \in \mathbb{R}^{N \times F}$ is a snapshot of the spatial observation at time t . The spatial is a sensor network \mathcal{G} consisting of N discrete nodes, and

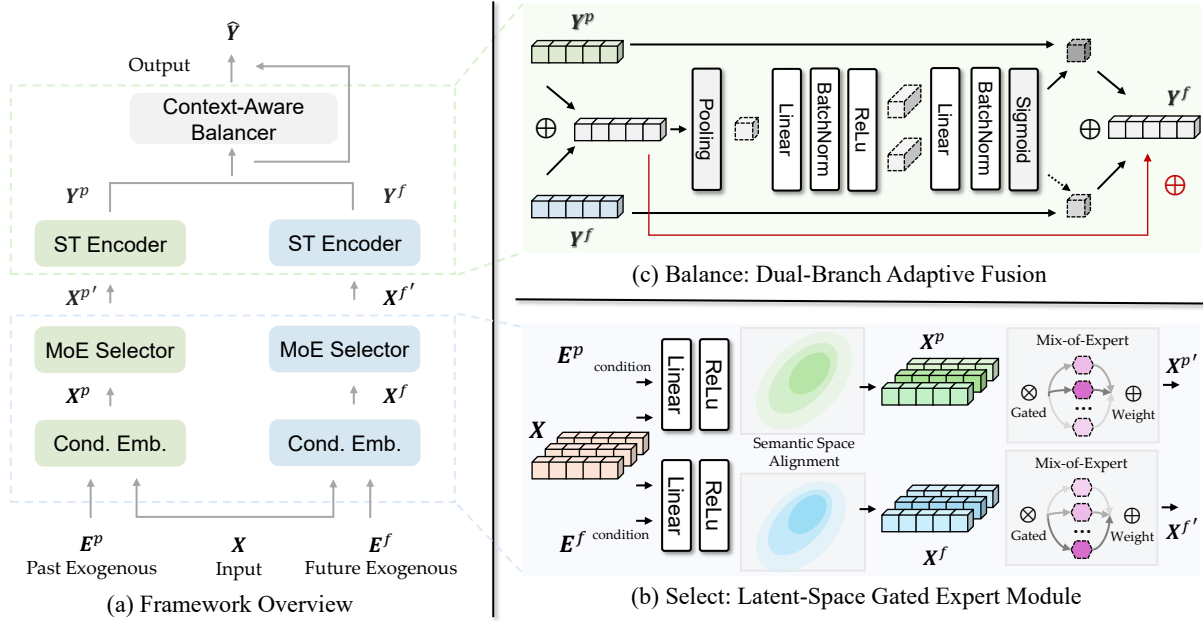


Figure 3: Overall framework of the proposed ExoST.

each node has F features at time t (e.g., pollutant indicators CO_2 , NO_2 , etc. from a dynamic air monitoring systems.).

DEFINITION 2. (Exogenous Variables). Exogenous variables are external system factors that are independent of the spatio-temporal forecasting and are free of the internal dynamics. During the modeling process, these variables are fed into the model as known inputs (whether actual observations or predicted values). Typically, these data hold the same structure as spatio-temporal data, denoted as $\mathcal{E} = \{E_t\}_{t=1}^T \sim \mathbb{P}$, and can be further subdivided into past exogenous variables (e.g., traffic flow and traffic speed at past moments) and future exogenous variables (e.g., future temperature and precipitation forecasts) according to their time attributes.

PROBLEM. (ST Forecasting with Exogenous Variables). Our goal is to learn an optimal prediction model for predicting future spatio-temporal signals from historical observations, optionally using exogenous inputs (and an optional graph structure prior \mathcal{G}). Let $\mathcal{D} = \{(\mathbf{X}_i, \mathbf{Y}_i)\}_{i=1}^{|\mathcal{D}|} \sim \mathbb{P}$ be a training dataset sampled from a spatio-temporal process, where $\mathbf{X}_i \in \mathbb{R}^{N \times T_p \times F}$ represents the features of N nodes for the past T_p time steps, and $\mathbf{Y}_i \in \mathbb{R}^{N \times T_f \times F}$ represents the target for the future T_f time steps. Traditional spatio-temporal prediction optimizes the model parameters θ^* by minimizing the expected prediction loss:

$$\theta^* = \arg \min_{\theta} \mathbb{E}_{(\mathbf{X}_i, \mathbf{Y}_i) \sim \mathbb{P}} [\mathcal{L}(f_{\theta}(\mathbf{X}_i, \mathcal{G}), \mathbf{Y}_i)],$$

where f_{θ} is the prediction model and \mathcal{L} measures the prediction error. When exogenous input $\mathbf{E}_i = (\mathbf{E}_i^{\text{past}}, \mathbf{E}_i^{\text{future}})$ is available, the goal becomes:

$$\theta^* = \arg \min_{\theta} \mathbb{E}_{(\mathbf{X}_i, \mathbf{E}_i, \mathbf{Y}_i) \sim \mathbb{P}} [\mathcal{L}(f_{\theta}(\mathbf{X}_i, \mathbf{E}_i, \mathcal{G}), \mathbf{Y}_i)],$$

where $\mathbf{E}_i^{\text{past}} \in \mathbb{R}^{N \times T_p \times F_p}$ and $\mathbf{E}_i^{\text{future}} \in \mathbb{R}^{N \times T_f \times F_f}$ denote the exogenous inputs in the past and future, respectively. F_p and F_f are the corresponding feature dimensions.

In practice, according to [25, 27, 46], the feature to be predicted is usually only the target variable, i.e., F in \mathbf{Y}_i is equal to 1.

3 METHODOLOGY

3.1 Overview

The ExoST is built on the “select-then-balance” paradigm, as shown in Figure 3. The process consists of two consecutive stages, which are used to address the two core challenges in exogenous-augmented spatio-temporal forecasting mentioned above: (i) inconsistent variable effects and (ii) unbalanced type effects.

- **Select stage (§3.2).** A lightweight Latent-Space Gated Expert module projects heterogeneous exogenous variables into a condition latent manifold, and then activates a Mixture-of-Experts Selector to dynamically re-weight and re-compose the most meaningful signals. The output is two refined, exogenous-aware representations $\mathbf{X}^{p'}$ and $\mathbf{X}^{f'}$, one for each type.

- **Balance stage (§3.3).** A Siamese dual-branch architecture processes the two representations in parallel through the existing spatio-temporal backbones, and a Context-Aware Balancer adaptively balances their contributions based on instantaneous context. The final forecast $\hat{\mathbf{Y}}$ is produced by a read-out layer on top of the fused hidden state.

Both stages are fully differentiable and backbone-agnostic: any modern ST encoder can be plugged in without architectural change.

3.2 Select: Latent-Space Gated Expert Module

The selection stage aims to address inconsistent variable effects by extract compact, adaptive semantic representations from input

endogenous variables and heterogeneous, multi-source exogenous variables, laying the foundation for the subsequent balancing stage. This requires a carefully designed two-step process: (i) semantic alignment of diverse exogenous and endogenous variables in a unified semantic space via conditional embeddings; (ii) adaptive selection through a mixture-of-experts selector that reweights and combines existing features to mitigate antagonism caused by inconsistent variable effects.

3.2.1 Conditional Embedding. Conditional embeddings specifically address the semantic space alignment of endogenous variables with two types of exogenous variables. For each exogenous type $\tau \in \{p, f\}$ (i.e., past, future), we first project the raw exogenous tensor $\mathbf{E}^\tau \in \mathbb{R}^{N \times T_\tau \times F_\tau}$ and the target history input $\mathbf{X} \in \mathbb{R}^{N \times T_p \times F}$ into a condition latent space via:

$$\mathbf{X}^\tau = \phi_{\text{cond}}^\tau(\mathbf{X}, \mathbf{E}^\tau), \quad (1)$$

where ϕ_{cond}^τ is implemented as affine-transformation block:

$$\phi_{\text{cond}}^\tau(\mathbf{X}, \mathbf{E}^\tau) = \text{Dropout}\left(\text{Act}\left(W_x^\tau \mathbf{X} + W_e^\tau \mathbf{E}^\tau + \mathbf{b}^\tau\right)\right), \quad (2)$$

where $W_x^\tau \in \mathbb{R}^{H \times F}$, $W_e^\tau \in \mathbb{R}^{H \times F_\tau}$ are learned projections that align heterogeneous feature dimensions into a latent semantic space. Specifically, consistent with common settings in existing literature [27, 46], the lengths of past and future steps are typically uniform. Therefore, to maintain this setting, we perform a direct element-wise add fusion. For more arbitrary cases, zero-padding preprocessing trick can also easily ensure alignment. Subsequently, non-linear activation functions project endogenous variables into latent conditional semantic spaces, derived from different types of exogenous variables, yielding conditional representations $\mathbf{X}^p \in \mathbb{R}^{N \times T \times H}$ and $\mathbf{X}^f \in \mathbb{R}^{N \times T \times H}$, respectively.

3.2.2 Mixture-of-Experts Selector. As discussed, inconsistent variable effects between exogenous and endogenous variables can induce antagonistic or synergistic semantic degeneration. This manifests as channel entanglement in the derived conditional representations, where semantic mixing may lead to rank-deficient representations, complicating the learning process. To address this, we attach a mixture-of-experts gating [18, 23, 48] module on top of each \mathbf{X}^τ . Concretely, we maintain K expert projections $\{W_k^\tau \in \mathbb{R}^{H \times H}\}_{k=1}^K$ and a gating network $\mathbf{g}^\tau : \mathbb{R}^H \rightarrow \Delta^K$ parameterized by a single linear layer followed by Softmax(\cdot) function. For each conditional representation input, the gating score $\mathbf{g}^\tau \in \mathbb{R}^K$ is applied at different time steps and locations and is calculated as follows:

$$\mathbf{g}^\tau = \text{Softmax}\left(W_g^\tau \mathbf{X}^\tau\right), \quad (3)$$

where W_g^τ is projection layer projection layer, along with a normalized activation function, calculates each expert's weight. This controls the weighting of each expert for the current input, simulating various semantic combinations. The final representation is then obtained through weighted combination:

$$\mathbf{X}^{\tau'} = \sum_{k=1}^K g_k^\tau W_k^\tau \mathbf{X}^\tau. \quad (4)$$

This strategy explicitly disentangles representations using a latent bottleneck and selective recombination, rather than forcing the model to learn entangled mappings. This latent space gating method

allows us to model multiple interactions between exogenous variables and the target representation within the fused conditional space, thereby adaptively acquiring suitable representation input $\mathbf{X}^{p'}$ and $\mathbf{X}^{f'}$ for the backbone network.

3.3 Balance: Dual-Branch Adaptive Fusion

The balancing stage aims to address the unbalanced type effect, that is, how to properly process the two semantic representations in the previous stage. This requires appropriately learning spatio-temporal dynamic patterns and effectively fusing them to achieve the final prediction. However, a key challenge arises from the inherent difference in temporal distribution between past and future exogenous information, complicating their effective fusion. To address this, we designed two crucial steps: (i) independent extraction of dynamic spatio-temporal features for both inputs via parallel siamese network branches. (ii) adaptive combination through a context-aware fusion gating mechanism that generates dynamic fusion weights to mitigate the imbalanced type effects.

3.3.1 Siamese ST Encoders. To effectively process the distinct characteristics of past- and future-conditioned semantic representations, we adopt a siamese architecture. This involves two identical spatio-temporal (ST) backbone encoders. Each encoder ϕ_{st}^τ , which can be instantiated with any existing spatio-temporal neural network [5, 19, 21, 30, 43, 56, 60], is tasked with capturing the complex spatial correlations and temporal dependencies within its respective input stream. The parallel processing yields two specialized representations:

$$\mathbf{Y}^\tau = \phi_{\text{st}}^\tau(\mathbf{X}^{\tau'}), \quad (5)$$

where $\mathbf{Y}^p \in \mathbb{R}^{N \times T_f \times 1}$ and $\mathbf{Y}^f \in \mathbb{R}^{N \times T_f \times 1}$ encapsulate the high-level spatio-temporal features derived from past and future exogenous contexts, respectively, preparing them for adaptive fusion.

3.3.2 Context-Aware Balancer. Simple fusion or weighted representations will not be able to adapt to dynamic changes in context. Therefore, the representations \mathbf{Y}^p and \mathbf{Y}^f are then integrated via a context-aware fusion gate that dynamically computes balancing weights. This gate learns to adjust the contribution of each branch based on the specific input instance, thereby mitigating the imbalance between noise and uncertainty. First, the two representations are element-wise add to form a unified context tensor $\mathbf{Y} = \mathbf{Y}^p + \mathbf{Y}^f$. An instance-specific gating signal α is then generated through a multi-step transformation:

$$\alpha = \sigma(\text{MLP}(\text{AvgPool}(\mathbf{Y}))), \quad (6)$$

where $\text{AvgPool}_N(\cdot)$ first aggregates spatial information to create a channel-wise descriptor. This descriptor is then passed through a bottleneck structure composed of two $\text{MLP}(\cdot)$ layers, with a ReLU non-linearity, and finally a Sigmoid activation $\sigma(\cdot)$ to produce the balancing weight α . The final prediction $\hat{\mathbf{Y}}$ is obtained by a weighted combination of the two branches, where α is broadcast appropriately:

$$\hat{\mathbf{Y}} = \alpha \odot \mathbf{Y}^p + (1 - \alpha) \odot \mathbf{Y}^f + \mathbf{Y}. \quad (7)$$

In addition, we also use the residual connection technique to supplement the context tensor to promote information propagation. This adaptive gating mechanism allows the model to dynamically prioritize past versus future information based on the input context,

effectively balancing their distinct type effects and producing a robust, fused result for prediction.

4 EXPERIMENTS

In this section, we conduct extensive experiments to investigate the following research questions:

- **RQ1:** Can **ExoST** outperform exogenous variable modeling methods in accuracy across various task scenarios? (*Effectiveness*)
- **RQ2:** Can **ExoST** achieve consistent improvements on various types of existing spatio-temporal backbones? (*Universality*)
- **RQ3:** Can **ExoST** maintain its performance in scenarios where exogenous variables are missing or noisy? (*Robustness*)
- **RQ4:** How does **ExoST** work? Which components or strategies are crucial? Are these components or strategies sensitive to different design or hyper-parameters? (*Mechanism*)
- **RQ5:** How does **ExoST** compare in efficiency and parameter count to other methods? (*Efficiency & Lightweight*)

4.1 Experimental Setup

Datasets. We conducted various experiments on two public real-world spatio-temporal datasets¹, which contains hourly measurements collected from monitoring stations in Madrid during the periods 1 January to 30 June 2019 and 1 January to 30 June 2022. Each dataset includes monitoring data from air quality, meteorological, and traffic systems. We consider four forecasting tasks: (i) *AQI-19* and *AQI-22*: predict NO_2 concentrations in air quality system using 2019 / 2022 data, with traffic and meteorological indicators as exogenous variables; (ii) *Speed-19* and *Intensity-22*: predict traffic speed / intensity in the traffic system using 2019 / 2022 data, with other system indicators as exogenous variables. All dataset are chronologically split into training, validation, and test sets in a 7:2:1 ratio. In addition, it is worth noting that we also include the coding of dates as both past and future exogenous variables as input. More details on dataset, please refer to Appendix A.1.

Baseline. For performance comparison, we categorize existing baselines into three groups: (i) time series models with exogenous variable modeling : TimeXer [53], TiDE [14], and NBEATSx [40]; (ii) spatio-temporal models with exogenous variable integration: MAGCRN [20]; (iii) general exogenous variable modeling frameworks: ChronosX [3], which allows for the substitution of any backbone. Additionally, to evaluate **ExoST**’s universality, we extensively utilize various classic spatio-temporal backbones, including AGCRN [5], GWNet [56], GGNN [43], GRUGCN [19], STGCN [60], and DCRNN [30]. More details on methods, see Appendix A.2.

Protocol. By default, we use the previous 24 steps of historical data to predict data for the next 24 steps (*i.e.*, 1-day), and evaluate using mean absolute error (MAE), root mean square error (RMSE), mean relative error (MRE), and mean absolute percentage error (MAPE). Moreover, to measure the long-term generalization of the model in real-world deployments, we also perform rolling evaluations over 2 and 3 days without retraining. For the baselines, we use the parameter settings recommended in their papers and fine-tune them. For **ExoST**, we set the number of gated experts to 4 and the hidden size to 64. To ensure fairness, each experiment is repeated five

times, and results are reported as the mean \pm standard deviation. Best results are highlighted in **bold pink** and the second-best in underlined blue. For more details on the protocol, see Appendix A.3.

4.2 Effectiveness Study (RQ1)

Table 1 shows the performance comparison of our model with various state-of-the-art methods for time series forecasting or spatio-temporal forecasting that utilize exogenous variable modeling. It is worth noting that the first three time series forecasting methods have coupled model designs, while MAGCRN, ChronosX, and our method all use classical AGCRN[5] as the backbone network to ensure a fair comparison. Our observations are as follows: ❶ Time series forecasting methods generally achieve the worst results, which is consistent with common spatio-temporal forecasting benchmarks [46]. This is because they generally do not consider spatial dependencies, resulting in inaccurate predictions. ❷ The ChronosX method, which utilizes a spatio-temporal backbone, despite achieving relative progress, often encounters non-convergence issues on some tasks during training (*i.e.*, *Speed-19* and *Intensity-22*). Despite repeated parameter tuning, this issue cannot be avoided. We attribute this to the design of the underlying Chronos-type [2] time series foundation model. ❸ MAGCRN often achieves suboptimal results because it is specifically designed for spatio-temporal prediction scenarios and still ignores the inconsistent and unbalanced effects of exogenous variables. ❹ Our **ExoST** achieves competitive performance across all metrics on the four tasks. By effectively selecting and balancing exogenous information, the **ExoST** can adapt to a variety of input sources, maintaining stable performance.

4.3 Universality Study (RQ2)

We further aim to demonstrate the universality of our **ExoST**’s “select, then balance” paradigm across various spatio-temporal backbones. Table 2 illustrates the performance improvements of our proposed **ExoST** for 3-day predictions across four tasks and six models. The ✖ column reflects the performance metrics of the backbone model alone on the target system, while the ✔ column displays the improved results achieved by our **ExoST** through exogenous variable modeling. The relative improvement is quantified in the Δ column. Based on these results, we make the following observations: ❶ Our **ExoST** exhibits significant performance improvements across different architectures and datasets, attributed to an effective exogenous variable modeling paradigm. ❷ From the model perspective, the extent of performance improvement varies among different backbone networks, with AGCRN yielding the optimal overall enhancement; however, even the least performing Gwnet model achieved substantial performance gains. ❸ From the task perspective, air quality prediction consistently showed stable performance improvements, as exogenous information like traffic and meteorology significantly impacts it; conversely, traffic speed prediction saw only moderate improvements due to the limited influence of exogenous information such as air quality. We further supplement results for 1- and 2-day predictions in Appendix B.1 and additionally find that ❹ as the prediction horizon extends, our **ExoST** achieves more significant gains, which also indicates the strong generalization capability of our method.

¹<https://zenodo.org/records/7308425>

Table 1: Comparison of the overall performance of advance methods and ExoST. For the *Speed-19* *, MAE and RMSE values are presented with a 10^2 scale to facilitate detailed comparison.

Datasets		AQI-19			Speed-19 *			AQI-22			Intensity-22		
Method	Metric	1-day	2-day	3-day	1-day	2-day	3-day	1-day	2-day	3-day	1-day	2-day	3-day
<i>TiDE</i> [14]	MAE	14.73 \pm 0.01	15.68 \pm 0.00	15.66 \pm 0.01	6.70 \pm 1.83	7.43 \pm 1.75	7.58 \pm 1.73	10.51 \pm 0.05	11.32 \pm 0.04	11.89 \pm 0.04	150.18 \pm 0.02	157.00 \pm 0.01	161.17 \pm 0.02
	RMSE	20.73 \pm 0.03	21.76 \pm 0.04	21.70 \pm 0.04	44.47 \pm 5.16	50.37 \pm 4.21	51.26 \pm 4.10	14.67 \pm 0.00	15.76 \pm 0.01	16.43 \pm 0.01	217.05 \pm 0.15	223.13 \pm 0.16	226.96 \pm 0.17
	MAPE (%)	93.01 \pm 0.53	98.80 \pm 0.43	98.60 \pm 0.41	16.38 \pm 4.62	18.02 \pm 4.42	18.37 \pm 4.36	87.51 \pm 0.98	95.07 \pm 0.93	99.22 \pm 0.92	146.50 \pm 0.03	147.09 \pm 0.07	150.07 \pm 0.06
	MRE (%)	56.96 \pm 0.04	60.67 \pm 0.01	60.67 \pm 0.02	17.44 \pm 4.78	19.33 \pm 4.56	19.72 \pm 4.51	56.27 \pm 0.24	60.56 \pm 0.20	63.62 \pm 0.20	54.43 \pm 0.01	56.82 \pm 0.00	58.21 \pm 0.01
<i>TimeXer</i> [53]	MAE	13.11 \pm 0.02	13.92 \pm 0.29	14.08 \pm 0.18	5.07 \pm 0.09	5.61 \pm 0.11	5.71 \pm 0.11	9.65 \pm 0.59	10.13 \pm 0.08	9.88 \pm 0.46	128.05 \pm 1.05	138.34 \pm 4.13	149.21 \pm 6.48
	RMSE	20.20 \pm 0.03	20.88 \pm 0.05	21.23 \pm 0.03	38.84 \pm 2.09	41.25 \pm 2.23	41.84 \pm 2.19	14.98 \pm 0.46	15.57 \pm 0.12	15.14 \pm 0.59	191.72 \pm 1.27	199.38 \pm 8.40	210.42 \pm 8.93
	MAPE (%)	64.48 \pm 0.27	65.90 \pm 4.25	68.33 \pm 3.68	12.42 \pm 0.51	13.67 \pm 0.55	13.93 \pm 0.55	63.07 \pm 7.20	66.30 \pm 3.65	65.05 \pm 2.85	191.61 \pm 3.61	188.09 \pm 1.44	190.11 \pm 0.93
	MRE (%)	50.71 \pm 0.08	53.93 \pm 1.11	54.49 \pm 0.68	13.20 \pm 0.24	14.59 \pm 0.29	14.86 \pm 0.29	51.64 \pm 3.13	54.21 \pm 0.40	52.86 \pm 2.47	46.41 \pm 0.34	49.96 \pm 2.01	53.88 \pm 2.67
<i>NBEATSx</i> [40]	MAE	11.63 \pm 0.08	13.88 \pm 0.06	14.10 \pm 0.09	5.21 \pm 0.30	5.99 \pm 0.29	6.17 \pm 0.28	8.13 \pm 0.11	9.71 \pm 0.19	9.97 \pm 0.17	38.91 \pm 1.68	67.02 \pm 1.78	85.03 \pm 1.43
	RMSE	18.44 \pm 0.04	20.65 \pm 0.06	21.20 \pm 0.04	39.56 \pm 2.02	45.80 \pm 2.23	46.80 \pm 2.20	12.84 \pm 0.08	14.84 \pm 0.19	15.02 \pm 0.19	70.08 \pm 4.91	117.62 \pm 2.98	141.30 \pm 1.92
	MAPE (%)	56.54 \pm 1.34	69.08 \pm 1.30	69.99 \pm 1.47	13.56 \pm 0.77	15.59 \pm 0.75	16.06 \pm 0.73	55.89 \pm 1.69	67.26 \pm 2.25	71.37 \pm 2.27	25.12 \pm 0.89	38.23 \pm 0.99	48.76 \pm 0.73
	MRE (%)	44.96 \pm 0.32	53.77 \pm 0.24	54.55 \pm 0.33	13.17 \pm 0.34	23.33 \pm 0.45	30.50 \pm 0.26	43.50 \pm 0.61	51.96 \pm 1.02	53.35 \pm 0.89	14.11 \pm 0.61	24.26 \pm 0.64	30.71 \pm 0.51
<i>MAGCRN</i> [20]	MAE	9.82 \pm 0.11	10.52 \pm 0.13	11.03 \pm 0.27	3.87 \pm 0.05	3.88 \pm 0.05	3.89 \pm 0.05	7.41 \pm 0.24	7.80 \pm 0.25	8.06 \pm 0.33	37.47 \pm 1.06	52.51 \pm 6.80	65.32 \pm 11.02
	RMSE	15.18 \pm 0.25	16.03 \pm 0.24	16.55 \pm 0.38	31.83 \pm 0.02	31.84 \pm 0.03	31.91 \pm 0.02	11.43 \pm 0.14	11.91 \pm 0.23	11.96 \pm 0.40	68.52 \pm 4.56	93.26 \pm 9.74	108.66 \pm 17.87
	MAPE (%)	38.56 \pm 0.27	42.53 \pm 0.41	45.08 \pm 1.15	9.41 \pm 0.07	9.43 \pm 0.08	9.44 \pm 0.08	43.79 \pm 4.21	45.89 \pm 4.35	49.74 \pm 4.19	20.12 \pm 0.26	27.20 \pm 2.58	34.88 \pm 4.66
	MRE (%)	37.97 \pm 0.44	40.69 \pm 0.50	42.72 \pm 1.03	10.08 \pm 0.13	10.08 \pm 0.13	10.09 \pm 0.13	39.66 \pm 1.30	41.74 \pm 1.34	43.15 \pm 1.77	13.58 \pm 0.38	19.00 \pm 2.46	23.59 \pm 3.98
<i>ChronosX</i> [3]	MAE	12.46 \pm 0.28	13.02 \pm 0.12	13.30 \pm 0.03	39.20 \pm 0.57	39.19 \pm 0.56	39.20 \pm 0.55	8.87 \pm 0.06	9.30 \pm 0.13	9.54 \pm 0.02	142.06 \pm 3.19	148.59 \pm 3.20	156.41 \pm 4.19
	RMSE	18.37 \pm 0.36	19.17 \pm 0.11	19.41 \pm 0.13	139.33 \pm 0.10	139.36 \pm 0.09	139.43 \pm 0.08	13.23 \pm 0.11	13.87 \pm 0.12	13.92 \pm 0.14	216.75 \pm 3.33	222.80 \pm 4.13	231.04 \pm 4.85
	MAPE (%)	55.86 \pm 0.72	59.48 \pm 1.72	60.74 \pm 2.43	99.50 \pm 0.44	99.54 \pm 0.44	99.58 \pm 0.42	58.84 \pm 2.39	61.46 \pm 2.74	65.24 \pm 2.63	58.60 \pm 3.79	64.23 \pm 1.65	69.75 \pm 1.09
	MRE (%)	48.17 \pm 1.08	50.39 \pm 0.49	51.53 \pm 0.13	102.00 \pm 1.52	101.98 \pm 1.46	101.98 \pm 1.41	47.49 \pm 0.34	49.78 \pm 0.71	51.07 \pm 0.11	51.35 \pm 0.92	53.78 \pm 1.16	56.49 \pm 1.52
<i>ExoST</i>	MAE	9.33 \pm 0.13	10.04 \pm 0.19	10.41 \pm 0.12	3.79 \pm 0.01	3.80 \pm 0.01	3.80 \pm 0.01	7.33 \pm 0.21	7.61 \pm 0.23	7.94 \pm 0.29	31.91 \pm 1.35	50.59 \pm 0.04	64.13 \pm 3.86
	RMSE	14.24 \pm 0.18	15.12 \pm 0.26	15.51 \pm 0.16	31.73 \pm 0.02	31.78 \pm 0.02	31.85 \pm 0.02	11.14 \pm 0.21	11.52 \pm 0.49	11.79 \pm 0.51	56.49 \pm 2.54	89.10 \pm 7.36	109.01 \pm 9.19
	MAPE (%)	38.57 \pm 0.32	42.62 \pm 0.52	44.65 \pm 0.08	9.30 \pm 0.03	9.32 \pm 0.03	9.31 \pm 0.03	44.90 \pm 0.88	46.59 \pm 0.64	50.27 \pm 1.18	17.63 \pm 0.97	26.68 \pm 1.69	34.52 \pm 2.90
	MRE (%)	36.09 \pm 0.49	38.84 \pm 0.75	40.34 \pm 0.47	9.88 \pm 0.03	9.89 \pm 0.03	9.90 \pm 0.03	39.23 \pm 1.11	40.74 \pm 1.24	42.50 \pm 1.57	11.57 \pm 0.49	18.31 \pm 1.14	23.16 \pm 1.40

Table 2: Performance comparison of different models w/ and w/o ExoST on common benchmarks (3-day scenario).

	Model	AGCRN			GWNet			GGNN			GRUGCN			STGCN			DCRNN		
		w/ ExoST	✗	✓	Δ(%)	✗	✓	Δ(%)	✗	✓	Δ(%)	✗	✓	Δ(%)	✗	✓	Δ(%)		
AQI-19	MAE	14.05 \pm 0.20	10.41 \pm 0.12	↓ 25.91	12.67 \pm 2.25	13.33 \pm 0.41	↑ 5.21	14.39 \pm 0.22	12.30 \pm 1.08	↓ 14.52	14.10 \pm 0.09	12.83 \pm 0.55	↓ 9.01	15.17 \pm 1.31	13.14 \pm 0.94	↓ 13.38	14.75 \pm 0.20	11.52 \pm 0.40	↓ 21.84
	RMSE	20.92 \pm 0.47	15.51 \pm 0.16	↓ 25.86	19.00 \pm 3.52	19.81 \pm 0.28	↑ 4.26	20.88 \pm 0.07	18.57 \pm 1.62	↓ 11.06	21.20 \pm 0.04	19.58 \pm 0.54	↓ 7.64	21.72 \pm 0.61	19.90 \pm 1.08	↓ 8.47	21.76 \pm 0.32	17.51 \pm 0.86	↓ 19.53
	MAPE(%)	63.79 \pm 1.32	44.65 \pm 0.08	↓ 30.00	63.50 \pm 2.08	62.43 \pm 3.94	↓ 1.68	73.36 \pm 1.23	53.55 \pm 8.41	↓ 27.00	69.99 \pm 1.47	50.96 \pm 2.82	↓ 27.20	82.69 \pm 20.81	57.21 \pm 7.64	↓ 30.70	73.64 \pm 4.33	46.56 \pm 2.39	↓ 36.81
	MRE(%)	54.36 \pm 0.77	40.34 \pm 0.47	↓ 25.79	54.05 \pm 0.50	51.65 \pm 1.60	↓ 4.44	56.39 \pm 1.93	47.67 \pm 4.20	↓ 15.46	54.55 \pm 0.33	49.71 \pm 1.15	↓ 8.87	58.89 \pm 2.27	50.91 \pm 3.66	↓ 13.67	57.09 \pm 0.78	44.62 \pm 1.55	↓ 21.84
Speed-19*	MAE	3.94 \pm 0.01	3.80 \pm 0.01	↓ 3.55	4.03 \pm 0.06	3.86 \pm 0.06	↓ 4.22	22.53 \pm 3.92	4.53 \pm 0.38	↓ 79.89	38.48 \pm 0.02	4.63 \pm 0.63	↓ 87.97	6.45 \pm 0.48	4.64 \pm 0.45	↓ 28.06	4.87 \pm 0.05	4.03 \pm 0.20	↓ 17.25
	RMSE	31.88 \pm 0.02	31.85 \pm 0.02	↓ 0.09	32.00 \pm 0.06	32.05 \pm 0.05	↑ 0.16	45.89 \pm 3.35	32.89 \pm 0.12	↓ 28.32	139.12 \pm 0.01	32.63 \pm 0.45	↓ 76.54	44.46 \pm 0.50	33.84 \pm 0.60	↓ 23.90	34.49 \pm 0.38	32.26 \pm 0.09	↓ 6.50
	MAPE(%)	9.42 \pm 0.03	9.31 \pm 0.03	↓ 1.17	9.54 \pm 0.23	9.65 \pm 0.23	↑ 1.14	14.15 \pm 0.27	10.63 \pm 0.18	↓ 24.90	99.86 \pm 0.01	10.67 \pm 0.50	↓ 89.33	14.02 \pm 0.46	11.20 \pm 0.81	↓ 20.11	11.70 \pm 0.14	9.73 \pm 0.20	↓ 16.84
	MRE(%)	10.21 \pm 0.02	9.90 \pm 0.03	↓ 3.04	10.49 \pm 0.52	10.05 \pm 0.16	↓ 4.20	58.60 \pm 10.19	11.78 \pm 0.69	↓ 79.90	100.09 \pm 0.05	12.04 \pm 1.78	↓ 87.97	16.60 \pm 1.03	12.06 \pm 0.92	↓ 27.35	12.68 \pm 0.13	10.49 \pm 0.34	↓ 17.27
AQI-22	MAE	10.19 \pm 0.21	7.94 \pm 0.29	↓ 22.08	10.05 \pm 0.04	9.11 \pm 0.12	↓ 9.35	10.44 \pm 0.04	8.82 \pm 0.14	↓ 15.51	9.97 \pm 0.17	8.58 \pm 0.19	↓ 13.96	10.65 \pm 0.60	9.21 \pm 0.11	↓ 13.51	10.33 \pm 0.72	7.70 \pm 0.34	↓ 25.47
	RMSE	15.34 \pm 0.02	11.79 \pm 0.51	↓ 23.14	15.11 \pm 0.27	13.66 \pm 0.08	↓ 9.60	15.13 \pm 0.04	13.01 \pm 0.25	↓ 14.03	15.02 \pm 0.19	13.29 \pm 0.43	↓ 11.51	15.65 \pm 0.50	14.16 \pm 0.17	↓ 9.53	15.25 \pm 0.83	11.81 \pm 0.61	↓ 22.49
	MAPE(%)	56.91 \pm 2.06	50.27 \pm 1.18	↓ 11.67	60.72 \pm 1.66	60.70 \pm 1.57	↓ 0.03	71.58 \pm 1.28	59.79 \pm 2.29	↓ 16.47	71.37 \pm 2.27	53.48 \pm 1.16	↓ 25.07	73.76 \pm 10.10	59.47 \pm 0.81	↓ 19.41	69.19 \pm 0.00	51.26 \pm 3.68	↓ 25.93
	MRE(%)	54.54 \pm 1.12	42.50 \pm 1.57	↓ 22.08	53.77 \pm 0.20	48.75 \pm 0.65	↓ 9.34	55.85 \pm 0.21	47.18 \pm 0.74	↓ 15.52	53.35 \pm 0.89	45.89 \pm 1.02	↓ 13.99	56.98 \pm 3.20	49.28 \pm 0.58	↓ 13.51	55.27 \pm 3.85	41.18 \pm 1.83	↓ 25.50
Intensity-22	MAE	85.76 \pm 0.47	64.13 \pm 3.86	↓ 25.22	87.34 \pm 0.75	61.87 \pm 3.80	↓ 29.14	84.17 \pm 0.43	77.29 \pm 15.21	↓ 8.17	85.03 \pm 1.43	75.55 \pm 6.83	↓ 11.16	90.49 \pm 0.75	72.17 \pm 1.54	↓ 20.23	87.57 \pm 0.79	64.55 \pm 2.61	↓ 26.29
	RMSE	144.77 \pm 0.94	109.01 \pm 9.19	↓ 28.34	147.13 \pm 1.61	105.44 \pm 5.53	↓ 28.34	141.73 \pm 1.35	125.02 \pm 25.74	↓ 11.83	141.30 \pm 1.92	122.13 \pm 11.30	↓ 13.62	148.09 \pm 0.05	117.47 \pm 1.89	↓ 20.68	145.99 \pm 1.77	109.83 \pm 2.77	↓ 24.49
	MAPE(%)	59.46 \pm 3.18	34.90 \pm 2.50	↓ 41.94	44.80 \pm 8.09	31.74 \pm 4.49	↓ 29.15	47.16 \pm 0.66	45.19 \pm 6.92	↓ 4.18	48.76 \pm 0.73	44.98 \pm 5.12	↓ 7.65	50.02 \pm 6.67	39.01 \pm 0.67	↓ 22.01	46.25 \pm 1.65	34.83 \pm 2.83	↓ 25.85
	MRE(%)	30.97 \pm 0.17	23.16 \pm 1.40	↓ 25.22	31.54 \pm 0.27	22.35 \pm 1.37	↓ 29.14	30.40 \pm 0.16	27.91 \pm 5.50	↓ 8.19	30.71 \pm 0.51	27.29 \pm 2.47	↓ 11.14	32.68 \pm 0.27	26.06 \pm 0.56	↓ 20.39	31.62 \pm 0.29	23.31 \pm 0.94	↓ 26.27

Table 3: Performance under abnormal conditions with missing exogenous variable signals (3-day scenario). For the *Speed-19* *, MAE and RMSE values are presented with a 10^2 scale to facilitate detailed comparison.

Datasets		AQI-19				Speed-19*				Intensity-22			
Masking Strategy		MAE	RMSE	MAPE(%)	MRE(%)	MAE	RMSE	MAPE(%)	MRE(%)	MAE	RMSE	MAPE(%)	MRE(%)
Zero	20%-Mask	10.60 \pm 0.15	15.87 \pm 0.16	44.83 \pm 1.39	41.07 \pm 0.60	3.87 \pm 0.03	31.94 \pm 0.06	9.47 \pm 1.20	10.08 \pm 0.90	64.31 \pm 9.49	108.23 \pm 18.00	34.19 \pm 3.45	23.23 \pm 3.43
	40%-Mask	11.33 \pm 0.02	17.07 \pm 0.09	46.13 \pm 1.45	43.91 \pm 0.09	3.89 \pm 0.07	31.98 \pm 0.08	9.53 \pm 1.80	10.12 \pm 1.60	67.80 \pm 1.82	115.25 \pm 3.73	38.21 \pm 0.21	24.49 \pm 0.65
	60%-Mask	11.44 \pm 0.52	17.30 \pm 0.84	48.30 \pm 2.02	44.34 \pm 2.01	3.87 \pm 0.05	31.96 \pm 0.09	9.48 \pm 1.50	10.08 \pm 1.40	68.50 \pm 10.78	118.41 \pm 17.47	36.37 \pm 6.38	24.74 \pm 3.89
	80%-Mask	12.33 \pm 0.00	18.94 \pm 0.00	52.03 \pm 0.00	47.79 \pm 0.00	3.83 \pm 0.02	31.89 \pm 0.06	9.40 \pm 0.90	9.95 \pm 0.50	69.70 \pm 10.99	118.51 \pm 18.88	38.18 \pm 6.62	25.17 \pm 3.97
Random	20%-Mask	10.67 \pm 0.16	16.17 \pm 0.19	44.23 \pm 2.37	41.32 \pm 0.62	3.86 \pm 0.03	31.94 \pm 0.08	9.44 \pm 1.40	10.05 \pm 1.00	67.32 \pm 8.42	114.89 \pm 16.03	34.88 \pm 3.82	24.32 \pm 3.04
	40%-Mask	11.30 \pm 0.08	17.09 \pm 0.23	46.57 \pm 1.19	43.78 \pm 0.32	3.84 \pm 0.02	31.92 \pm 0.04	9.42 \pm 0.60	9.99 \pm 0.50	64.43 \pm 10.78	110.41 \pm 17.43	34.34 \pm 7.21	23.27 \pm 3.89
	60%-Mask	11.37 \pm 0.05	17.26 \pm 0.22	47.43 \pm 1.15	44.04 \pm 0.18	3.87 \pm 0.05	31.95 \pm 0.09	9.49 \pm 1.40	10.06 \pm 1.40	65.27 \pm 6.06	109.81 \pm 11.90	35.34 \pm 3.27	23.57 \pm 2.19
	80%-Mask	12.33 \pm 0.00	18.94 \pm 0.00	52.03 \pm 0.00	47.79 \pm 0.00	3.88 \pm 0.05	31.93 \pm 0.09	9.48 \pm 1.60	10.08 \pm 1.20	68.13 \pm 10.61	115.96 \pm 18.89	36.61 \pm 4.61	24.60 \pm 3.83
No Masking		10.41 \pm 0.12	15.51 \pm 0.16	42.62 \pm 0.52	38.84 \pm 0.75	3.80 \pm 0.01	31.85 \pm 0.02	9.31 \pm 0.03	9.90 \pm 0.03	64.13 \pm 3.86	109.01 \pm 9.19	34.52 \pm 2.90	23.16 \pm 1.40

can be viewed as a simple data augmentation strategy. By introducing different data perturbations, the model is forced to learn to predict under a variety of incomplete or noisy data conditions, thereby enhancing its generalization and robustness. We also provide a performance comparison for the 1-day and 2-day scenarios in Appendix B.2, observing similar results.

4.5 Mechanism Study (RQ4)

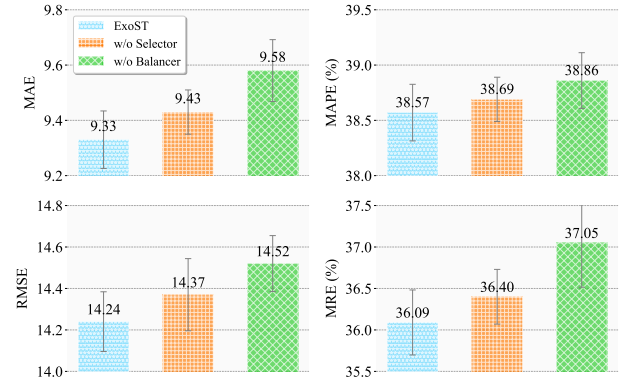
4.5.1 Ablation Study. We first conducted an ablation study to systematically evaluate the impact of different components on ExoST from two perspectives: data input and model component.

From the data perspective, we aimed to investigate the auxiliary role of different types of exogenous variables in the final prediction. Specifically, due to the universality of date information, here, we treated it as a separate category. As shown in Table 4, we observed that ❶ future exogenous variables outperformed past, indicating that forward-looking information provides more direct predictive signals. However, combining both past and future yielded better performance than using either type alone, which suggests that the combination can provide complementary patterns. ❷ We also found that date exogenous variables performed poorly when used in isolation but led to improvements when combined with any other type. ❸ Best performance was achieved by combining all exogenous variables. This demonstrates that ExoST can effectively exploit different information, extracting and balancing contributions from different temporal perspectives and contextual information.

From the model perspective, we aimed to investigate the auxiliary role of different module components in the final prediction.

Table 4: Ablation study from the data perspective on AQI-19 for 1-day forecasting, where P, F, and D represent Past, Future, and Data exogenous variables respectively.

P	F	D	MAE	RMSE	MAPE (%)	MRE (%)
✓	-	-	13.09 \pm 0.65	19.35 \pm 0.52	65.54 \pm 5.87	50.64 \pm 2.50
-	✓	-	9.97 \pm 0.36	15.09 \pm 0.52	41.20 \pm 1.97	38.56 \pm 1.38
-	-	✓	12.47 \pm 0.15	19.15 \pm 0.20	57.42 \pm 5.11	48.21 \pm 0.58
✓	-	✓	12.20 \pm 0.09	18.72 \pm 0.08	59.06 \pm 1.72	47.16 \pm 0.33
-	✓	✓	9.63 \pm 0.00	14.69 \pm 0.00	39.68 \pm 0.03	37.24 \pm 0.02
✓	✓	-	9.69 \pm 0.33	14.93 \pm 0.59	39.42 \pm 0.69	37.46 \pm 1.28
✓	✓	✓	9.33 \pm 0.13	14.24 \pm 0.18	38.57 \pm 0.32	36.09 \pm 0.49

**Figure 4: Ablation study on AQI-19 comparing ExoST, w/ Selector, and w/ Balancer variants in 1-day forecasting horizons.**

We constructed two variants by removing the MoE Selector and the Context-aware Balancer (achieved through direct element-wise fusion), respectively. As Figure 9 shows, ❶ w/ Selector variant significantly degrades performance in all metrics, demonstrating the critical importance of addressing inconsistent variable effects. Performance degradation indicates that without proper semantic alignment and adaptive selection mechanisms, the model struggles to disentangle heterogeneous exogenous variables from endogenous variables, leading to feature space competition and channel entanglement issues. ❷ w/ Balancer variant causes even more pronounced performance degradation than w/ Selector variant, highlighting that temporal distribution differences between past and future exogenous information pose a more fundamental challenge, requiring sophisticated balancing mechanisms to handle noise-contaminated past information and uncertainty-amplified future forecasts.

More experimental results are shown in Appendix B.3.1.

4.5.2 Parameter Study. We then conducted a parameter study to evaluate the impact of different parameter on ExoST. As Figure 5 shows, we can observe that ❶ The hidden size of 64 achieves optimal performance in all prediction horizons, with larger sizes leading to performance degradation due to overfitting. ❷ Expert number of 4 provides the best balance between model capacity and computational efficiency. Too few experts (one or two) fail to capture the diverse semantic patterns needed for disentangling inconsistent variable effects, while excessive experts (eight) lead to overselection

where redundant experts compete for similar patterns, diminishing the effectiveness of the mixture-of-experts gating mechanism designed to mitigate channel entanglement. These observations validate the effectiveness of our lightweight design choices in the latent-space gated expert module.

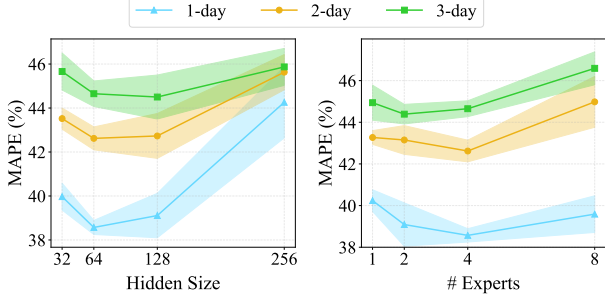


Figure 5: MAPE performance comparison on AQI-19 dataset for different hyperparameter settings: hidden size and the number of experts across 1, 2, and 3-day forecasting horizons.

4.5.3 Strategy Study. We also use several alternative strategies to test the rationality of our design. These include: (i) *Shared Parameter*: Two siamese branches share parameters to learn a unified spatio-temporal representation. (ii) *Simple Weight*: Adopts a predefined balancing weight ($\alpha = 0.5$) to fuse the outputs from two siamese branches. (iii) *Learnable Weight*: Dynamically adjusts the relative importance of past and future information through learnable parameters. (iv) *Attention*: Utilizes cross-attention mechanisms to dynamically balance the contributions from two siamese branches. As shown in Figure 6, we observe that: ❶ **ExoST** achieves competitive performance in other strategies, demonstrating the effectiveness of our design choice. ❷ *Simple Weight* shows significant performance degradation due to its static balancing strategy that does not adapt to varying input contexts. ❸ *Attention* and *Learnable*

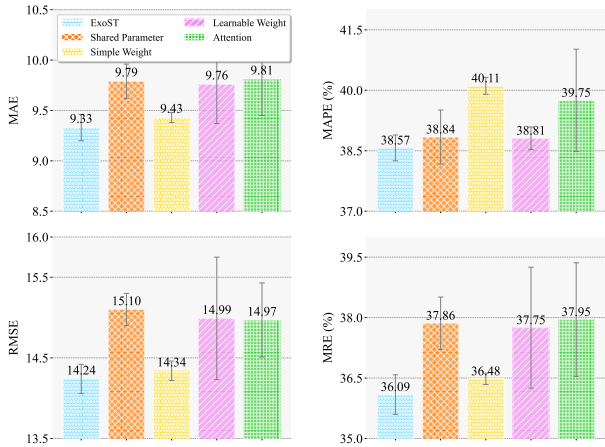


Figure 6: Different strategy performance comparison on AQI-19 dataset comparing ExoST, share parameter, simple weight, learned parameter and attention variants on 1-day scenario.

Weight strategies underperform while increasing computational complexity, as attention mechanisms introduce excessive parameter overhead and learnable weights lack the sophisticated context modeling capabilities needed to handle nuanced differences between exogenous variables of the past and future. More experimental results are shown in Appendix B.3.2.

4.6 Efficiency & Lightweight Study (RQ5)

We compared the differences in *training time*, *memory footprint*, and *performance* between **ExoST** and other time series or spatio-temporal forecasting models that incorporate exogenous variables on the AQI-19 dataset. Due to varying convergence epochs, for a fair comparison, we only present the average training time for the first 100 epochs. As shown in Figure 7, compared to several other methods, **ExoST** demonstrates a balance of performance, efficiency, and model parameter count. Furthermore, we can observe that: ❶ compared to time series models with different backbones, despite its lightweight model design, it leads to poor performance. ❷ compared to spatio-temporal method and the general exogenous variables modeling method with the same backbone (*i.e.*, MAGCRN, ChronosX), we achieved further performance improvement while maintaining similar parameters and training time.

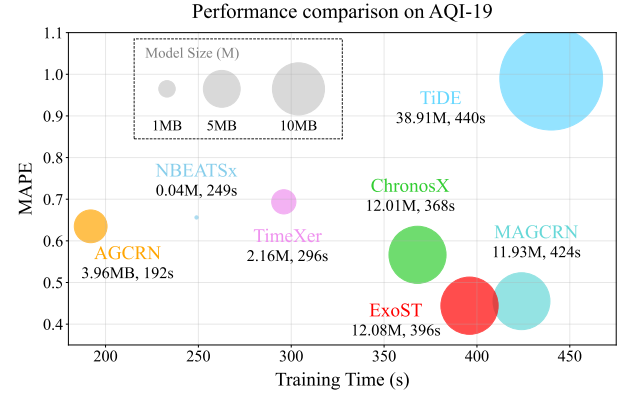


Figure 7: Efficiency & Lightweight Study on AQI-19 dataset comparing training efficiency (first 100 epochs) and 3-day MAPE across different models.

5 CONCLUSION AND FUTURE WORK

This paper investigates the challenges of modeling exogenous variables for spatio-temporal forecasting and explores effective implementation options. We propose a novel framework, **ExoST**, which follows a “select, then balance” paradigm. It first dynamically selects and restructures salient signals via a latent space gated expert module to address inconsistent variable effects. It then incorporates a dual-branch architecture with a context-aware weighting mechanism to address imbalanced type effects. Extensive experiments demonstrate its effectiveness, universality, and robustness. In future work, we aim to explore how to broaden the modal availability of exogenous variables and their feasibility in data-scarce scenarios.

REFERENCES

- [1] 2024. Position: What can large language models tell us about time series analysis. In *41st International Conference on Machine Learning*. MLResearchPress.
- [2] Abdul Fatir Ansari, Lorenzo Stella, Ali Caner Turkmen, Xiyuan Zhang, Pedro Mercado, Huibin Shen, Aleksandr Shchur, Syama Sundar Rangapuram, Sebastian Pineda Arango, Shubham Kapoor, et al. [n. d.]. Chronos: Learning the Language of Time Series. *Transactions on Machine Learning Research* ([n. d.]).
- [3] Sebastian P Arango, Pedro Mercado, Shubham Kapoor, Ashish F Ansari, Laurent Stella, Hong Shen, and Syama Sundar Rangapuram. 2025. ChronosX: Adapting pretrained time series models with exogenous variables. *arXiv preprint arXiv:2503.12107* (2025).
- [4] Allan M Avila and Igor Mezić. 2020. Data-driven analysis and forecasting of highway traffic dynamics. *Nature communications* 11, 1 (2020), 2090.
- [5] Lei Bai, Lina Yao, Can Li, Xianjie Wang, and Chunrong Wang. 2020. Adaptive graph convolutional recurrent network for traffic forecasting. In *Advances in neural information processing systems*, Vol. 33. 17804–17815.
- [6] Safaa Berkani, Bassma Guermah, Mehdi Zakroum, and Mounir Ghogho. 2023. Spatio-temporal forecasting: A survey of data-driven models using exogenous data. *IEEE Access* 11 (2023), 75191–75214.
- [7] Kaifeng Bi, Lingxi Xie, Hengheng Zhang, Xin Chen, Xiaotao Gu, and Qi Tian. 2023. Accurate medium-range global weather forecasting with 3D neural networks. *Nature* 619, 7970 (2023), 533–538.
- [8] Bahar Biller and Barry L Nelson. 2003. Modeling and generating multivariate time-series input processes using a vector autoregressive technique. *ACM Transactions on Modeling and Computer Simulation (TOMACS)* 13, 3 (2003), 211–237.
- [9] George EP Box and David A Pierce. 1970. Distribution of residual autocorrelations in autoregressive-integrated moving average time series models. *Journal of the American statistical Association* 65, 332 (1970), 1509–1526.
- [10] Lingxiao Cao, Bin Wang, Guiyuan Jiang, Yanwei Yu, and Junyu Dong. 2025. Spatiotemporal-aware Trend-Seasonality Decomposition Network for Traffic Flow Forecasting. In *Proceedings of the AAAI Conference on Artificial Intelligence*, Vol. 39. 11463–11471.
- [11] Ching Chang, Wei-Yao Wang, Wen-Chih Peng, and Tien-Fu Chen. 2025. Llm4ts: Aligning pre-trained llms as data-efficient time-series forecasters. *ACM Transactions on Intelligent Systems and Technology* 16, 3 (2025), 1–20.
- [12] Wei Chen and Yuxuan Liang. 2025. Expand and Compress: Exploring Tuning Principles for Continual Spatio-Temporal Graph Forecasting. In *The Thirteenth International Conference on Learning Representations*.
- [13] Wei Chen and Yuxuan Liang. 2025. Learning with Calibration: Exploring Test-Time Computing of Spatio-Temporal Forecasting. *arXiv preprint arXiv:2506.00635* (2025).
- [14] Abhimanyu Das, Weihao Kong, Andrew Leach, Shaan Mathur, Rajat Sen, and Rose Yu. 2023. Long-term forecasting with tide: Time-series dense encoder. *arXiv preprint arXiv:2304.08424* (2023).
- [15] Chengxiang Dong, Xiaoliang Feng, Yongchao Wang, and Xin Wei. 2023. Spatiotemporal exogenous variables enhanced model for traffic flow prediction. *IEEE Access* 11 (2023), 95958–95973.
- [16] Wei Fan, Shun Zheng, Pengyang Wang, Rui Xie, Kun Yi, Qi Zhang, Jiang Bian, and Yanjie Fu. 2025. In-flow: Instance normalization flow for non-stationary time series forecasting. In *Proceedings of the 31st ACM SIGKDD Conference on Knowledge Discovery and Data Mining V. 1*. 295–306.
- [17] Yuchen Fang, Hao Miao, Yuxuan Liang, Liwei Deng, Yue Cui, Ximu Zeng, Yuyang Xia, Yan Zhao, Torben Bach Pedersen, Christian S Jensen, et al. 2025. Unraveling Spatio-Temporal Foundation Models via the Pipeline Lens: A Comprehensive Review. *arXiv preprint arXiv:2506.01364* (2025).
- [18] William Fedus, Barret Zoph, and Noam Shazeer. 2022. Switch transformers: Scaling to trillion parameter models with simple and efficient sparsity. *Journal of Machine Learning Research* 23, 120 (2022), 1–39.
- [19] Jiaxin Gao and Bruno Ribeiro. 2022. On the equivalence between temporal and static equivariant graph representations. In *International Conference on Machine Learning*. PMLR, 7052–7076.
- [20] Antonio Giganti, Sara Mandelli, Paolo Bestagini, Umberto Giuriato, Alessandro D’Ausilio, Marco Marcon, and Stefano Tubaro. 2024. Back to the Future: GNN-Based No 2 Forecasting Via Future Covariates. In *IGARSS 2024-2024 IEEE International Geoscience and Remote Sensing Symposium*. IEEE, 3872–3876.
- [21] Shengnan Guo, Youfang Lin, Ning Feng, Chao Song, and Huaiyu Wan. 2019. Attention based spatial-temporal graph convolutional networks for traffic flow forecasting. In *Proceedings of the AAAI conference on artificial intelligence*, Vol. 33. 922–929.
- [22] Qihe Huang, Zhengyang Zhou, Kuo Yang, and Yang Wang. 2025. Exploiting Language Power for Time Series Forecasting with Exogenous Variables. In *Proceedings of the ACM on Web Conference* 2025. 4043–4052.
- [23] Robert A Jacobs, Michael I Jordan, Steven J Nowlan, and Geoffrey E Hinton. 1991. Adaptive mixtures of local experts. *Neural computation* 3, 1 (1991), 79–87.
- [24] Furong Jia, Kevin Wang, Yixiang Zheng, Defu Cao, and Yan Liu. 2024. Gpt4mts: Prompt-based large language model for multimodal time-series forecasting. In *Proceedings of the AAAI Conference on Artificial Intelligence*, Vol. 38. 23343–23351.
- [25] Guangyin Jin, Yuxuan Liang, Yuchen Fang, Zezhi Shao, Jincai Huang, Junbo Zhang, and Yu Zheng. 2023. Spatio-temporal graph neural networks for predictive learning in urban computing: A survey. *IEEE Transactions on Knowledge and Data Engineering* 36, 10 (2023), 5388–5408.
- [26] Ming Jin, Huan Yee Koh, Qingsong Wen, Daniele Zambon, Cesare Alippi, Geoffrey I Webb, Irwin King, and Shirui Pan. 2023. A survey on graph neural networks for time series: Forecasting, classification, imputation, and anomaly detection. *arXiv preprint arXiv:2307.03759* (2023).
- [27] Ming Jin, Huan Yee Koh, Qingsong Wen, Daniele Zambon, Cesare Alippi, Geoffrey I Webb, Irwin King, and Shirui Pan. 2024. A survey on graph neural networks for time series: Forecasting, classification, imputation, and anomaly detection. *IEEE Transactions on Pattern Analysis and Machine Intelligence* (2024).
- [28] Ming Jin, Shiyu Wang, Lintao Ma, Zhixuan Chu, James Y Zhang, Xiaoming Shi, Pin-Yu Chen, Yuxuan Liang, Yuan-Fang Li, Shirui Pan, et al. [n. d.]. Time-LLM: Time Series Forecasting by Reprogramming Large Language Models. In *The Twelfth International Conference on Learning Representations*.
- [29] Weiyang Kong, Ziyu Guo, and Yubao Liu. 2024. Spatio-temporal pivotal graph neural networks for traffic flow forecasting. In *Proceedings of the AAAI conference on artificial intelligence*, Vol. 38. 8627–8635.
- [30] Yaguang Li, Rose Yu, Cyrus Shahabi, and Yan Liu. 2017. Diffusion convolutional recurrent neural network: Data-driven traffic forecasting. *arXiv preprint arXiv:1707.01926* (2017).
- [31] Zhonghang Li, Lianghao Xia, Jiabin Tang, Yong Xu, Lei Shi, Long Xia, Dawei Yin, and Chao Huang. 2024. Urbangpt: Spatio-temporal large language models. In *Proceedings of the 30th ACM SIGKDD Conference on Knowledge Discovery and Data Mining*. 5351–5362.
- [32] Yuxuan Liang, Yutong Xia, Songyu Ke, Yiwei Wang, Qingsong Wen, Junbo Zhang, Yu Zheng, and Roger Zimmermann. 2023. Airformer: Predicting nationwide air quality in china with transformers. In *Proceedings of the AAAI Conference on Artificial Intelligence*, Vol. 37. 14329–14337.
- [33] Johan Lindström, Adam A Szpiro, Paul D Sampson, Assaf P Oron, Mark Richards, Tim V Larson, and Lianne Sheppard. 2014. A flexible spatio-temporal model for air pollution with spatial and spatio-temporal covariates. *Environmental and ecological statistics* 21 (2014), 411–433.
- [34] Chenxi Liu, Kethmi Hirushini Hettige, Qianxiong Xu, Cheng Long, Shili Xiang, Gao Cong, Ziyue Li, and Rui Zhao. 2025. ST-LLM+: Graph Enhanced Spatio-Temporal Large Language Models for Traffic Prediction. *IEEE Transactions on Knowledge and Data Engineering* (2025).
- [35] Chenxi Liu, Qianxiong Xu, Hao Miao, Sun Yang, Lingzheng Zhang, Cheng Long, Ziyue Li, and Rui Zhao. 2025. Timecma: Towards llm-empowered multivariate time series forecasting via cross-modality alignment. In *Proceedings of the AAAI Conference on Artificial Intelligence*, Vol. 39. 18780–18788.
- [36] Chenxi Liu, Sun Yang, Qianxiong Xu, Zhishuai Li, Cheng Long, Ziyue Li, and Rui Zhao. 2024. Spatial-temporal large language model for traffic prediction. In *2024 25th IEEE International Conference on Mobile Data Management (MDM)*. IEEE, 31–40.
- [37] Hangchen Liu, Zheng Dong, Renhe Jiang, Jiewen Deng, Jinliang Deng, Qun-jun Chen, and Xuan Song. 2023. Spatio-temporal adaptive embedding makes vanilla transformer sota for traffic forecasting. In *Proceedings of the 32nd ACM international conference on information and knowledge management*. 4125–4129.
- [38] Minbo Ma, Kai Tang, Huan Li, Fei Teng, Dalin Zhang, and Tianrui Li. 2025. Beyond Fixed Variables: Expanding-variate Time Series Forecasting via Flat Scheme and Spatio-temporal Focal Learning. *Proceedings of the 31st ACM SIGKDD Conference on Knowledge Discovery and Data Mining* (2025).
- [39] Yuqi Nie, Nam H Nguyen, Phanwadee Sinthong, and Jayant Kalagnanam. 2023. A Time Series is Worth 64 Words: Long-term Forecasting with Transformers. In *The Eleventh International Conference on Learning Representations*.
- [40] Kin G Olivares, Cristian Challu, Grzegorz Marcjasz, Rafał Weron, and Artur Dubrawski. 2023. Neural basis expansion analysis with exogenous variables: Forecasting electricity prices with NBEATs. *International Journal of Forecasting* 39, 2 (2023), 884–900.
- [41] Zijie Pan, Yushan Jiang, Sahil Garg, Anderson Schneider, Yuriy Nemvyvaka, and Dongjin Song. 2024. s² IP-LLM: Semantic space informed prompt learning with LLM for time series forecasting. In *Forty-first International Conference on Machine Learning*.
- [42] Xiangfei Qiu, Xingjian Wu, Yan Lin, Chenjuan Guo, Jilin Hu, and Bin Yang. 2025. Duet: Dual clustering enhanced multivariate time series forecasting. In *Proceedings of the 31st ACM SIGKDD Conference on Knowledge Discovery and Data Mining V. 1*. 1185–1196.
- [43] Victor G Satorras, Syama Sundar Rangapuram, and Tim Januschowski. 2022. Multivariate time series forecasting with latent graph inference. *arXiv preprint arXiv:2203.03423* (2022).
- [44] Hyunwoo Seo and Chiehyeon Lim. 2025. ST-MTM: Masked Time Series Modeling with Seasonal-Trend Decomposition for Time Series Forecasting. In *Proceedings of the 31st ACM SIGKDD Conference on Knowledge Discovery and Data Mining V. 1*. 1209–1220.
- [45] Zezhi Shao, Fei Wang, Yongjun Xu, Wei Wei, Chengqing Yu, Zhao Zhang, Di Yao, Guangyin Jin, Xin Cao, Gao Cong, et al. 2023. Exploring Progress in Multivariate Time Series Forecasting: Comprehensive Benchmarking and Heterogeneity

- Analysis. *arXiv preprint arXiv:2310.06119* (2023).
- [46] Zezhi Shao, Fei Wang, Yongjun Xu, Wei Wei, Chengqing Yu, Zhao Zhang, Di Yao, Tao Sun, Guangyin Jin, Xin Cao, et al. 2024. Exploring progress in multivariate time series forecasting: Comprehensive benchmarking and heterogeneity analysis. *IEEE Transactions on Knowledge and Data Engineering* (2024).
 - [47] Zezhi Shao, Zhao Zhang, Fei Wang, Wei Wei, and Yongjun Xu. 2022. Spatial-temporal identity: A simple yet effective baseline for multivariate time series forecasting. In *Proceedings of the 31st ACM international conference on information & knowledge management*. 4454–4458.
 - [48] Noam Shazeer, Azalia Mirhoseini, Krzysztof Maziarczyk, Andy Davis, Quoc Le, Geoffrey Hinton, and Jeff Dean. 2017. Outrageously large neural networks: The sparsely-gated mixture-of-experts layer. *arXiv preprint arXiv:1701.06538* (2017).
 - [49] Chenxi Sun, Hongyan Li, Yaliang Li, and Shenda Hong. [n. d.]. TEST: Text Prototype Aligned Embedding to Activate LLM’s Ability for Time Series. In *The Twelfth International Conference on Learning Representations*.
 - [50] Mingtian Tan, Mike Merrill, Vinayak Gupta, Tim Althoff, and Tom Hartvigsen. 2024. Are language models actually useful for time series forecasting? *Advances in Neural Information Processing Systems* 37 (2024), 60162–60191.
 - [51] Stylianos I Vagropoulos, Gi Choularas, Evangelos G Kardakos, Christos K Simoglou, and Anastasios G Bakirtzis. 2016. Comparison of SARIMAX, SARIMA, modified SARIMA and ANN-based models for short-term PV generation forecasting. In *2016 IEEE international energy conference (ENERGYCON)*. IEEE, 1–6.
 - [52] Shuo Wang, Yanran Li, Jiang Zhang, Qingye Meng, Lingwei Meng, and Fei Gao. 2020. Pm2.5-gnn: A domain knowledge enhanced graph neural network for pm2.5 forecasting. In *Proceedings of the 28th international conference on advances in geographic information systems*. 163–166.
 - [53] Yuxuan Wang, Haixu Wu, Jiaxiang Dong, Guo Qin, Haoran Zhang, Yong Liu, Yunzhong Qiu, Jianmin Wang, and Mingsheng Long. 2024. Timexer: Empowering transformers for time series forecasting with exogenous variables. *arXiv preprint arXiv:2402.19072* (2024).
 - [54] Billy M Williams. 2001. Multivariate vehicular traffic flow prediction: evaluation of ARIMAX modeling. *Transportation Research Record* 1776, 1 (2001), 194–200.
 - [55] Haixu Wu, Tengge Hu, Yong Liu, Hang Zhou, Jianmin Wang, and Mingsheng Long. 2022. Timesnet: Temporal 2d-variation modeling for general time series analysis. In *The Eleventh International Conference on Learning Representations*. arXivpreprint.
 - [56] Zonghan Wu, Shirui Pan, Guodong Long, Jing Jiang, and Chengqi Zhang. 2019. Graph wavenet for deep spatial-temporal graph modeling. *arXiv preprint arXiv:1906.00121* (2019).
 - [57] Kaiwen Xia, Li Lin, Shuai Wang, Qi Zhang, Shuai Wang, and Tian He. 2025. ProST: Prompt Future Snapshot on Dynamic Graphs for Spatio-Temporal Prediction. In *Proceedings of the 31st ACM SIGKDD Conference on Knowledge Discovery and Data Mining V. 1*. 1645–1656.
 - [58] Yiwu Xu and Mengchi Liu. 2025. GPT4TFP: Spatio-temporal fusion large language model for traffic flow prediction. *Neurocomputing* 625 (2025), 129562.
 - [59] Xiaosong Yang, Thomas L Delworth, Liwei Jia, Nathaniel C Johnson, Feiyu Lu, and Colleen McHugh. 2024. Skillful seasonal prediction of wind energy resources in the contiguous United States. *Communications Earth & Environment* 5, 1 (2024), 313.
 - [60] Bing Yu, Haoteng Yin, and Zhanxing Zhu. 2017. Spatio-temporal graph convolutional networks: A deep learning framework for traffic forecasting. *arXiv preprint arXiv:1709.04875* (2017).
 - [61] Athanassios Zagouras, Hugo TC Pedro, and Carlos FM Coimbra. 2015. On the role of lagged exogenous variables and spatio-temporal correlations in improving the accuracy of solar forecasting methods. *Renewable Energy* 78 (2015), 203–218.
 - [62] Pengfei Zhou, Yunlong Liu, Junli Liang, Qi Song, and Xiangyang Li. 2025. CrossLinear: Plug-and-Play Cross-Correlation Embedding for Time Series Forecasting with Exogenous Variables. *arXiv preprint arXiv:2505.23116* (2025).

SUPPLEMENTARY MATERIAL

SELECT, THEN BALANCE: A PLUG-AND-PLAY FRAMEWORK FOR
EXOGENOUS-AWARE SPATIO-TEMPORAL FORECASTING

TABLE OF CONTENTS

A Experimental Details	11
A.1 Datasets Details	11
A.2 Baseline Details	11
A.3 Protocol Details	12
B More Results	12
B.1 More Result on Universality Study	12
B.2 More Result on Robustness Study	13
B.3 More Result on Mechanism Study	13
C More Disscuison	15
C.1 Limitation	15
C.2 Future Direction	16

A EXPERIMENTAL DETAILS

A.1 Datasets Details

The statistics of the two real-world datasets used in this paper are summarized in Table 5.

Table 5: Summary of datasets used for our experiments. M: million (10^6).

Attribute	Madrid-19	Madrid-22
Time range	01/01/2019 – 30/06/2019	01/01/2022 – 30/06/2022
Frames	4344	4344
Sampling Rate	1 hour	1 hour
Data points	2.03 M	2.03 M
Variables	20	20
Variable Domain	Air quality, Traffic, Meteorological, Date	Air quality, Traffic, Meteorological, Date

Graph Construction for GNN-based Models. We classify the GNN models into *adaptive graph construction* and *predefined graph structure* based on their graph construction approaches and perform graph construction on datasets accordingly. For *adaptive graph construction* models including AGCRN, GraphWaveNet, GGNN, and MAGCRN, the adjacency matrix $\mathbf{A} \in \mathbb{R}^{N \times N}$ is computed by embedding the learnable node. Specifically, given node embeddings $\mathbf{E} \in \mathbb{R}^{N \times d_e}$ where d_e is the embedding dimension, AGCRN computes the adjacency matrix as $\mathbf{A} = \text{softmax}(\text{ReLU}(\mathbf{E}\mathbf{E}^T))$, where $\mathbf{E}\mathbf{E}^T$ computes the similarity between all pairs of nodes, ReLU ensures non-negative similarities, and softmax normalizes the weights to create a valid adjacency matrix. This approach allows the model to automatically discover the latent spatial dependencies between the monitoring stations without requiring prior knowledge of their geographical relationships. GWNet uses separate source \mathbf{E}_s and

target embeddings \mathbf{E}_t to compute the adjacency matrix as $\mathbf{A} = \text{softmax}(\text{ReLU}(\mathbf{E}_s\mathbf{E}_t^T))$, allowing more flexible spatial relationship modeling. GGNN employs a fully connected graph structure where $\mathbf{A}_{ij} = 1$ for all $i, j \in \{1, 2, \dots, N\}$, enabling dense spatial attention across all pairs of node. MAGCRN inherits the adaptive graph construction capability from AGCRN, automatically learning the graph structure through node embeddings. For *predefined graph structure* models that include STGCN, DCRNN, and GRUGCN, due to the lack of geographic location, we follow the mainstream practice² and construct the adjacency matrix based on the Pearson correlation coefficient of the target time series. Given the target variable $\mathbf{X}_t \in \mathbb{R}^{N \times F}$ at time t , we compute the correlation matrix $\mathbf{C} \in \mathbb{R}^{N \times N}$ where $C_{ij} = \rho_{ij}$ represents the Pearson correlation coefficient between nodes i and j . The adjacency matrix is then constructed as $\mathbf{A}_{ij} = \begin{cases} \rho_{ij}, & \text{if } j \in \text{TopK}(\rho_{i,:}) \\ 0, & \text{otherwise} \end{cases}$, where the *TopK* operation retains the k most correlated connections for each node, specifically choosing $k = 8$.

Variable Scales and Units. For the *AQI-19* and *AQI-22*, the target variable NO_2 ranges from 0 to 328 $\mu\text{g}/\text{m}^3$ in Madrid-19 and 0 to 625 $\mu\text{g}/\text{m}^3$ in Madrid-22, with mean values of 36.6 and 28.0 $\mu\text{g}/\text{m}^3$ respectively. For the *Speed-19* and *Intensity-22*, the target variables have various scales: the average traffic speed in Madrid-19 ranges from 0 to 3.57 km/h with a mean of approximately 1.2 km/h , while the traffic intensity in Madrid-22 ranges from 56.5 to 289.88 vehicles/hour with a mean of approximately 170 vehicles/hour. Traffic variables show substantial scale differences: traffic intensity ranges from 56 to 429 *vehicles/hour*, traffic occupation time varies from 0.5% to 5.76%, traffic load ranges from 6.5% to 28.12%, and traffic average speed ranges from 0 to 3.57 km/h . Exogenous variables maintain consistent scales across all tasks, with meteorological variables serving as future covariates and traffic variables (excluding the target) serving as past covariates. To handle these diverse scales effectively, we apply StandardScaler normalization to all variables, ensuring that each variable has zero mean and unit variance.

Temporal Variable Encoding. We employ consistent temporal encoding in four forecasting tasks using sinusoidal transformations for periodic features and one-hot encoding for categorical information. For continuous periodic features, given a timestamp t , the hour encoding is calculated as $\sin(2\pi \cdot \text{hour}(t)/24)$ and $\cos(2\pi \cdot \text{hour}(t)/24)$, and the month encoding as $\sin(2\pi \cdot (\text{month}(t) - 1)/12)$ and $\cos(2\pi \cdot (\text{month}(t) - 1)/12)$. For categorical temporal information, each weekday is represented as a binary vector $\mathbf{w} \in \{0, 1\}^7$, where $w_i = 1$ if the day corresponds to the i -th day of the week (Monday=0, Sunday=6), and $w_i = 0$ otherwise. These temporal features are added as *universal exogenous* variables to four tasks.

A.2 Baseline Details

In this appendix, we provide detailed descriptions of the advanced exogenous variable modeling methods and different spatio-temporal backbone models used in our default evaluation.

A.2.1 Exogenous Variable Modeling Methods. These methods are grouped into three main categories based on their approach to handling exogenous variables.

²Torch-Spatiotemporal

TS Models w/ Exogenous Variable Integration.

- *TiDE* [14]: *TiDE* is an encoder-decoder model built on multi-layer perceptrons (MLPs) that fuses historical time-series data and covariates via dense MLP residual blocks to map them into low-dimensional representations, then generates forecast sequences by incorporating future covariates. <https://github.com/google-research/google-research/tree/master/tide>
- *TimeXer* [53]: *TimeXer* is a Transformer model tailored for time series forecasting with exogenous variables: it captures temporal dependencies in the endogenous series via patch-level self-attention and effectively integrates exogenous information through variable-level cross attention and learnable global endogenous tokens to produce high-quality predictions of the target series. <https://github.com/thuml/TimeXer>
- *NBEATSx* [40]: *NBEATSx* extends the original N-BEATS by incorporating convolutional encoding substructures for time-varying and static exogenous variables within a hierarchical stacked residual block architecture, enabling interpretable decomposition of trend, seasonality, and exogenous factors for high-quality target-series forecasting. <https://github.com/cchallu/nbeatsx>

ST Models w/ Exogenous Variable Integration.

- *MAGCRN* [20]: *MAGCRN* is a spatio-temporal model that extends AGCRN into a dual-path architecture, using separate AGCRN blocks to encode historical observations and future exogenous covariates. <https://github.com/polimi-ispl/MAGCRN>

General Exogenous Variable Integration Framework.

- *ChronosX* [3]: *ChronosX* extends *MAGCRN* by integrating two exogenous adaptation modules: Instance-wise Interpolation Block (IIB) and Offset Integration Block (OIB). IIB adaptively interpolates exogenous inputs across time steps, while OIB injects time-dependent bias offsets into the output layer, enabling more flexible integration of future covariates. Due to the limited public availability of the code, we implemented the IIB and OIB modules based on the formulas provided in the referenced paper. <https://github.com/amazon-science/chronos-forecasting/tree/chronosx>

A.2.2 Spatio-Temporal Backbone Models. To ensure fair use of these models, we use a popular spatio-temporal forecasting benchmark library: <https://github.com/TorchSpatiotemporal/tsl>.

- *AGCRN* [5]: *AGCRN* is an adaptive graph-based recurrent model that captures fine-grained spatio-temporal dependencies by jointly learning node-specific patterns and data-driven graph structures, eliminating the need for pre-defined adjacency matrices.
- *GWNet* [56]: *GWNet* is a spatial-temporal model that combines diffusion-based graph convolutions with dilated causal temporal convolutions, and incorporates a learnable self-adaptive

adjacency matrix to capture latent spatial relationships from data.

- *GGNN* [43]: *GGNN* is a recurrent graph-based model that applies gated update mechanisms to iteratively refine node representations through message passing, enabling effective modeling of long-range structural dependencies.
- *GRUGCN* [19]: *GRUGCN* is a spatio-temporal neural architecture that integrates graph convolutions for spatial feature extraction and gated recurrent units for sequential modeling, effectively capturing dynamic dependencies in traffic forecasting scenarios.
- *STGCN* [60]: *STGCN* is a graph-based temporal forecasting model that integrates graph convolutional layers with temporal convolution modules to jointly learn spatial and temporal dependencies in structured time series data.
- *DCRNN* [30]: *DCRNN* is a graph-based recurrent forecasting model that captures spatial dependencies via diffusion convolutions on directed graphs and models temporal dynamics through a sequence-to-sequence recurrent architecture.

A.3 Protocol Details

A.3.1 Metrics Detail. We use different metrics such as MAE, RMSE, MRE, and MAPE. Formally, these metrics are formulated as follows:

$$\begin{aligned} \text{MAE} &= \frac{1}{n} \sum_{i=1}^n |y_i - \hat{y}_i|, & \text{RMSE} &= \sqrt{\frac{1}{n} \sum_{i=1}^n (y_i - \hat{y}_i)^2}, \\ \text{MRE} &= \frac{\sum_{i=1}^n |y_i - \hat{y}_i|}{\sum_{i=1}^n |y_i|}, & \text{MAPE} &= \frac{100\%}{n} \sum_{i=1}^n \left| \frac{\hat{y}_i - y_i}{y_i} \right|, \end{aligned}$$

where n represents the indices of all observed samples, y_i denotes the i -th actual sample and \hat{y}_i is the corresponding prediction. The mean relative error is defined as the MAE divided by the ℓ_1 norm of the target window.

A.3.2 Parameter Detail. The model is trained for 500 epochs using the AdamW optimizer with a cosine annealing learning rate scheduler. The learning rate is initialized at 10^{-2} and decays to 10^{-7} over the training period. A batch size of 512 is used, incorporating mixed-precision arithmetic and Z-score normalization for target variables. Early stopping is implemented to prevent overfitting, halting training if the validation MAE does not improve for 30 consecutive epochs. All experiments are carried out on a Linux server equipped with a $1 \times$ AMD EPYC 7763 128-Core Processor CPU with 256GB memory and $4 \times$ NVIDIA RTX A6000 GPUs, each with 48GB memory.

B MORE RESULTS

B.1 More Result on Universality Study

We provide more experimental results on universality (*i.e.*, for 1-day and 2-day scenarios), as shown in Tables 6 and 7. We observe that while the *ExoST* exhibits some negative gains in the 1-day scenario, it exhibits improved performance as the prediction length increases, demonstrating the superior generalization of our method.

Table 6: Performance comparison of different models w/ and w/o ExoST on common benchmarks on 1-Day Scenario.

Model		AGCRN			GWNet			GGNN			GRUGCN			STGCN			DCRNN		
w/ ExoST		✗	✓	Δ(%)	✗	✓	Δ(%)	✗	✓	Δ(%)	✗	✓	Δ(%)	✗	✓	Δ(%)	✗	✓	Δ(%)
AQI-19	MAE	13.63 \pm 0.45	9.33 \pm 0.13	↓ 31.55	10.92 \pm 0.01	11.57 \pm 0.32	↑ 5.95	11.57 \pm 0.37	10.78 \pm 0.48	↓ 6.83	11.63 \pm 0.08	11.65 \pm 0.39	↑ 0.17	13.60 \pm 1.30	11.55 \pm 0.21	↓ 15.07	13.80 \pm 0.46	10.25 \pm 0.19	↓ 25.72
	RMSE	20.43 \pm 0.89	14.24 \pm 0.18	↓ 30.30	17.17 \pm 3.31	17.79 \pm 0.37	↑ 3.61	18.25 \pm 0.20	16.87 \pm 0.89	↓ 7.56	18.44 \pm 0.04	18.43 \pm 0.38	↓ 0.05	20.56 \pm 1.21	18.30 \pm 0.29	↓ 10.99	21.07 \pm 0.43	16.28 \pm 0.06	↓ 22.73
	MAPE(%)	60.71 \pm 0.41	38.57 \pm 0.32	↓ 36.80	51.54 \pm 2.00	51.92 \pm 2.89	↑ 0.74	56.99 \pm 1.81	45.09 \pm 5.46	↓ 20.88	56.54 \pm 1.34	44.86 \pm 2.08	↓ 20.78	68.55 \pm 12.26	48.33 \pm 3.28	↓ 29.50	68.45 \pm 7.25	44.68 \pm 0.81	↓ 34.72
	MRE(%)	52.74 \pm 1.81	35.85 \pm 0.71	↓ 32.03	46.47 \pm 0.65	44.73 \pm 1.23	↓ 3.74	45.17 \pm 0.99	41.67 \pm 1.67	↓ 7.75	44.96 \pm 0.32	45.06 \pm 1.52	↑ 0.22	52.59 \pm 5.03	44.68 \pm 0.81	↓ 15.04	53.37 \pm 1.80	39.63 \pm 0.74	↓ 25.75
Speed-19*	MAE	3.92 \pm 0.01	3.79 \pm 0.01	↓ 3.32	3.81 \pm 0.13	3.70 \pm 0.06	↓ 2.89	21.81 \pm 3.90	4.03 \pm 0.26	↓ 81.52	38.45 \pm 0.02	4.39 \pm 0.68	↓ 88.60	5.53 \pm 0.40	4.34 \pm 0.36	↓ 21.52	4.52 \pm 0.05	3.81 \pm 0.13	↓ 15.71
	RMSE	31.78 \pm 0.02	31.73 \pm 0.02	↓ 0.16	30.92 \pm 0.04	31.42 \pm 0.04	↑ 1.61	43.31 \pm 3.43	31.08 \pm 0.12	↓ 28.30	139.01 \pm 0.01	31.76 \pm 0.45	↓ 77.15	38.60 \pm 0.65	32.19 \pm 0.60	↓ 16.61	32.47 \pm 0.12	31.11 \pm 0.09	↓ 4.19
	MAPE(%)	9.42 \pm 0.00	9.30 \pm 0.03	↓ 1.27	8.59 \pm 0.21	9.27 \pm 0.21	↑ 7.33	12.86 \pm 0.31	9.42 \pm 0.18	↓ 26.75	99.84 \pm 0.01	10.12 \pm 0.50	↓ 89.87	12.19 \pm 0.57	10.55 \pm 0.81	↓ 13.45	10.95 \pm 0.13	9.25 \pm 0.20	↓ 15.52
	MRE(%)	10.20 \pm 0.02	9.88 \pm 0.03	↓ 3.14	9.91 \pm 0.16	9.64 \pm 0.16	↓ 2.72	56.77 \pm 10.14	10.48 \pm 0.69	↓ 81.52	100.07 \pm 0.05	11.42 \pm 1.78	↓ 87.59	14.38 \pm 1.03	11.30 \pm 0.92	↓ 21.42	11.76 \pm 0.12	9.91 \pm 0.34	↓ 15.73
AQI-22	MAE	9.55 \pm 0.24	7.33 \pm 0.21	↓ 23.25	8.58 \pm 0.41	7.98 \pm 0.19	↓ 6.99	8.60 \pm 0.01	8.15 \pm 0.11	↓ 5.23	8.13 \pm 0.11	7.55 \pm 0.09	↓ 7.13	9.17 \pm 0.88	7.99 \pm 0.14	↓ 12.87	9.11 \pm 1.32	6.81 \pm 0.30	↓ 25.25
	RMSE	14.58 \pm 0.48	11.14 \pm 0.21	↓ 23.59	13.44 \pm 0.62	12.26 \pm 0.10	↓ 8.78	13.20 \pm 0.12	12.43 \pm 0.25	↓ 5.83	12.84 \pm 0.08	12.17 \pm 0.29	↓ 5.22	13.86 \pm 0.77	12.65 \pm 0.12	↓ 8.73	13.97 \pm 1.56	10.72 \pm 0.58	↓ 23.26
	MAPE(%)	31.80 \pm 0.70	44.90 \pm 0.88	↑ 41.19	49.43 \pm 1.83	51.38 \pm 1.95	↑ 3.94	55.74 \pm 1.04	53.39 \pm 2.41	↓ 4.21	55.89 \pm 1.69	45.92 \pm 1.50	↓ 17.76	61.74 \pm 11.81	50.05 \pm 2.16	↓ 18.93	59.84 \pm 11.34	43.94 \pm 3.49	↓ 26.57
	MRE(%)	51.10 \pm 1.28	39.23 \pm 1.11	↓ 23.23	45.94 \pm 1.19	42.69 \pm 1.02	↓ 7.07	46.01 \pm 0.06	43.63 \pm 0.60	↓ 5.17	43.50 \pm 0.61	40.41 \pm 0.50	↓ 7.10	49.06 \pm 4.70	42.76 \pm 0.75	↓ 12.84	48.77 \pm 7.09	36.44 \pm 1.62	↓ 25.30
Intensity-22	MAE	33.25 \pm 0.83	31.91 \pm 1.35	↓ 4.03	34.00 \pm 3.74	35.94 \pm 4.97	↑ 5.71	29.74 \pm 1.21	42.17 \pm 0.48	↑ 41.86	38.91 \pm 1.68	42.04 \pm 3.37	↑ 8.04	43.06 \pm 0.92	45.77 \pm 0.15	↑ 6.29	35.91 \pm 2.16	32.78 \pm 2.80	↓ 8.72
	RMSE	56.56 \pm 0.99	56.49 \pm 2.54	↓ 0.12	57.40 \pm 4.89	63.08 \pm 8.58	↑ 9.90	48.88 \pm 1.95	68.39 \pm 1.71	↑ 39.91	70.08 \pm 4.91	68.89 \pm 5.45	↓ 1.70	69.51 \pm 0.85	77.07 \pm 2.32	↑ 10.88	60.87 \pm 4.59	58.63 \pm 4.43	↓ 3.68
	MAPE(%)	18.53 \pm 0.75	17.63 \pm 0.97	↓ 4.86	17.78 \pm 1.97	20.28 \pm 3.36	↑ 14.06	19.26 \pm 0.95	22.95 \pm 0.95	↑ 19.16	25.12 \pm 0.89	24.94 \pm 2.91	↓ 0.72	24.23 \pm 1.85	25.15 \pm 2.09	↑ 3.79	19.88 \pm 2.19	17.71 \pm 1.93	↓ 10.91
	MRE(%)	12.05 \pm 0.30	11.57 \pm 0.49	↓ 3.98	12.32 \pm 1.36	13.03 \pm 1.80	↑ 5.76	10.78 \pm 0.44	15.28 \pm 0.18	↑ 41.74	14.11 \pm 0.61	15.24 \pm 1.22	↑ 7.96	15.61 \pm 0.33	16.59 \pm 0.06	↑ 6.28	13.01 \pm 0.78	11.89 \pm 1.01	↓ 8.61

Table 7: Performance comparison of different models w/ and w/o ExoST on common benchmarks(2-Day Scenario).

Model		AGCRN			GWNet			GGNN			GRUGCN			STGCN			DCRNN		
w/ ExoST		✗	✓	Δ(%)	✗	✓	Δ(%)	✗	✓	Δ(%)	✗	✓	Δ(%)	✗	✓	Δ(%)	✗	✓	Δ(%)
AQI-19	MAE	13.77 \pm 0.47	10.04 \pm 0.19	↓ 27.09	12.29 \pm 2.45	12.75 \pm 0.21	↑ 3.74	14.28 \pm 0.11	12.14 \pm 1.08	↓ 14.99	13.88 \pm 0.06	12.58 \pm 0.55	↓ 9.37	14.73 \pm 0.66	12.78 \pm 0.64	↓ 13.24	14.27 \pm 0.31	11.31 \pm 0.01	↓ 20.74
	RMSE	20.54 \pm 0.58	15.12 \pm 0.26	↓ 26.39	18.87 \pm 3.73	19.18 \pm 0.13	↑ 1.64	20.81 \pm 0.38	18.45 \pm 1.51	↓ 11.34	20.65 \pm 0.06	19.47 \pm 0.50	↓ 5.71	21.80 \pm 0.56	19.66 \pm 0.67	↓ 9.82	20.97 \pm 0.36	17.55 \pm 0.26	↓ 16.31
	MAPE(%)	62.14 \pm 0.54	42.62 \pm 0.52	↓ 31.41	60.03 \pm 4.32	58.83 \pm 2.95	↓ 2.00	71.16 \pm 1.37	52.19 \pm 0.62	↓ 26.66	69.08 \pm 1.30	49.74 \pm 2.81	↓ 27.99	75.40 \pm 9.03	54.59 \pm 0.32	↓ 27.61	70.18 \pm 0.64	43.76 \pm 0.03	↓ 37.65
	MRE(%)	53.33 \pm 1.79	38.84 \pm 0.75	↓ 27.17	52.24 \pm 1.39	49.36 \pm 0.82	↓ 5.51	55.63 \pm 0.78	46.97 \pm 4.17	↓ 15.58	53.77 \pm 0.24	48.68 \pm 2.11	↓ 9.47	57.02 \pm 2.55	49.45 \pm 2.46	↓ 13.28	55.27 \pm 1.22	43.76 \pm 0.03	↓ 20.82
Speed-19*	MAE	3.93 \pm 0.01	3.80 \pm 0.01	↓ 3.31	3.96 \pm 0.06	3.77 \pm 0.06	↓ 4.80	22.33 \pm 3.90	4.28 \pm 0.34	↓ 80.83	38.45 \pm 0.02	4.52 \pm 0.62	↓ 88.27	6.27 \pm 0.53	4.51 \pm 0.41	↓ 28.07	4.73 \pm 0.06	3.96 \pm 0.18	↓ 16.28
	RMSE	31.82 \pm 0.02	31.78 \pm 0.02	↓ 0.13	31.38 \pm 0.02	31.66 \pm 0.02	↑ 0.88	45.19 \pm 3.38	32.18 \pm 0.34	↓ 28.79	139.01 \pm 0.01	32.26 \pm 0.55	↓ 76.78	43.66 \pm 0.77	33.12 \pm 0.96	↓ 31.82	33.64 \pm 0.41	31.92 \pm 0.25	↓ 5.11
	MAPE(%)	9.43 \pm 0.02	9.32 \pm 0.03	↓ 1.17	9.05 \pm 0.23	9.45 \pm 0.22	↑ 4.76	13.82 \pm 0.29	10.03 \pm 0.35	↓ 27.42	99.85 \pm 0.01	10.44 \pm 0.70	↓ 89.55	13.59 \pm 0.58	10.94 \pm 0.91	↓ 19.49	11.41 \pm 0.14	9.58 \pm 0.30	↓ 16.04
	MRE(%)	10.21 \pm 0.02	9.89 \pm 0.03	↓ 3.13	10.29 \pm 0.46	9.83 \pm 0.15	↓ 4.68	58.11 \pm 10.16	11.13 \pm 0.88	↓ 80.84	100.08 \pm 0.05	11.77 \pm 1.61	↓ 88.24	16.09 \pm 1.11	11.75 \pm 1.05	↓ 26.97	12.32 \pm 0.16	10.29 \pm 0.46	↓ 16.48
AQI-22	MAE	9.91 \pm 0.05	7.61 \pm 0.23	↓ 23.21	9.39 \pm 0.20	8.66 \pm 0.17	↓ 7.78	10.10 \pm 0.03	8.49 \pm 0.17	↓ 15.94	9.71 \pm 0.19	8.10 \pm 0.07	↓ 16.57	10.00 \pm 0.76	8.71 \pm 0.14	↓ 12.90	9.93 \pm 0.85	7.35 \pm 0.21	↓ 25.97
	RMSE	15.08 \pm 0.12	11.52 \pm 0.49	↓ 23.61	14.51 \pm 0.34	13.26 \pm 0.04	↓ 8.60	14.93 \pm 0.12	12.76 \pm 0.18	↓ 14.52	14.84 \pm 0.19	13.07 \pm 0.23	↓ 11.91	14.98 \pm 0.65	13.77 \pm 0.21	↓ 8.08	14.85 \pm 0.89	11.47 \pm 0.39	↓ 22.79
	MAPE(%)	54.78 \pm 1.05	46.59 \pm 0.64	↓ 14.95	54.79 \pm 0.39	56.45 \pm 2.25	↑ 3.03	66.35 \pm 1.23	55.59 \pm 2.78	↓ 16.19	67.26 \pm 2.25	48.14 \pm 1.33	↓ 28.40	68.35 \pm 11.56	54.35 \pm 1.09	↓ 20.43	66.35 \pm 8.27	47.63 \pm 3.59	↓ 28.21
	MRE(%)	53.01 \pm 0.29	40.74 \pm 1.24	↓ 23.15	50.25 \pm 1.09	46.35 \pm 0.92	↓ 7.76	54.05 \pm 0.16	45.41 \pm 0.93	↓ 15.97	51.96 \pm 1.02	43.35 \pm 0.36	↓ 16.56	53.51 \pm 4.08	46.59 \pm 0.76	↓ 12.92	53.11 \pm 4.55	39.35 \pm 1.11	↓ 25.94
Intensity-22	MAE	62.66 \pm 0.59	50.59 \pm 0.04	↓ 19.26	62.65 \pm 1.19	51.09 \pm 4.57	↓ 18.53	61.34 \pm 0.83	62.36 \pm 10.83	↑ 1.66	67.02 \pm 1.78	62.31 \pm 1.14	↓ 7.04	68.04 \pm 0.65	60.90 \pm 1.19	↓ 10.49	64.29 \pm 1.37	50.53 \pm 3.94	↓ 21.39
	RMSE	113.21 \pm 1.13	89.10 \pm 7.36	↓ 21.30	113.12 \pm 1.07	91.20 \pm 7.36	↓ 19.38	111.50 \pm 0.40	102.84 \pm 19.01	↓ 7.78	117.62 \pm 2.98	104.07 \pm 6.46	↓ 11.53	116.81 \pm 0.13	102.06 \pm 2.49	↓ 12.63	114.56 \pm 2.74	90.24 \pm 6.35	↓ 21.23
	MAPE(%)	45.87 \pm 0.60	26.68 \pm 1.69	↓ 41.84	30.77 \pm 0.48	26.62 \pm 3.11	↓ 13.50	33.47 \pm 0.86	35.00 \pm 4.54	↑ 4.56	38.23 \pm 0.99	35.81 \pm 1.34	↓ 6.33	36.08 \pm 2.07	32.27 \pm 1.58	↓ 10.54	32.31 \pm 1.36	26.11 \pm 2.67	↓ 19.18
	MRE(%)	22.68 \pm 0.21	18.31 \pm 1.14	↓ 19.27	22.68 \pm 0.43	18.49 \pm 1.66	↓ 18.48	22.20 \pm 0.30	22.57 \pm 3.92	↑ 1.67	24.26 \pm 0.64	22.55 \pm 1.14	↓ 7.04	24.63 \pm 0.24	22.04 \pm 0.43	↓ 10.51	23.27 \pm 0.49	18.29 \pm 1.43	↓ 21.41

The remaining observations show similar analytical results to those in the main text.

B.2 More Result on Robustness Study

We provide more experimental results on robustness (*i.e.*, for 1-day and 2-day scenarios) in Tables 8 and 9. We observe similar analysis as in the main text.

B.3 More Result on Mechanism Study

B.3.1 Ablation Study. From the data perspective, we also evaluated the impact of exogenous variables on ExoST’s performance for 2-day and 3-day forecasting on the *AQI-19*, as shown in Tables 10 and Tables 11. We have

Table 8: Performance under missing values on 1-day scenario.

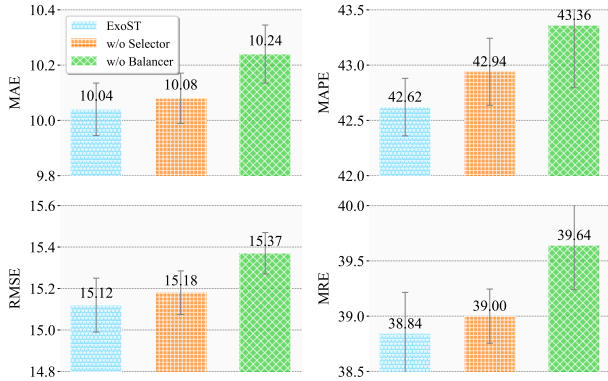
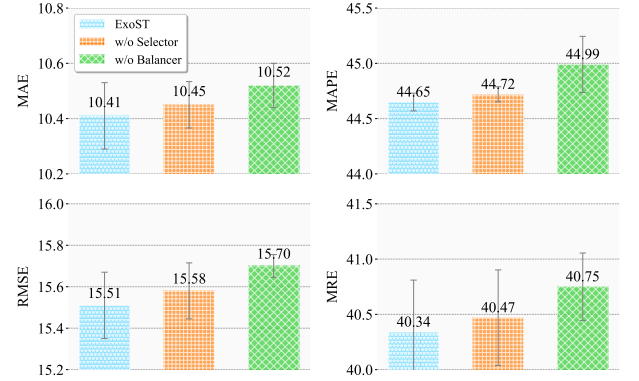
Datasets		AQI-19				Speed-19*				Intensity-22			
Masking Strategy		MAE	RMSE	MAPE(%)	MRE(%)	MAE	RMSE	MAPE(%)	MRE(%)	MAE	RMSE	MAPE(%)	MRE(%)
Zero	20%-Mask	9.98±0.24	15.19±0.06	40.86±0.02	38.59±0.01	3.81±0.01	31.80±0.04	9.28±0.01	9.91±0.01	33.74±3.24	62.25±7.82	17.81±1.15	12.23±1.18
	40%-Mask	10.41±0.26	16.22±0.52	41.00±0.34	40.28±1.03	3.79±0.01	31.77±0.02	9.23±0.01	9.84±0.01	33.70±0.40	58.59±2.51	19.63±0.77	12.22±0.14
	60%-Mask	10.33±0.22	16.26±0.56	41.71±0.01	39.98±0.01	3.80±0.01	31.75±0.05	9.31±0.15	9.90±0.12	36.22±0.39	65.67±3.71	19.90±0.68	13.13±0.14
	80%-Mask	10.99±0.15	17.10±0.29	47.36±4.28	42.50±0.58	3.81±0.03	31.78±0.06	9.41±0.13	9.93±0.08	35.96±1.23	64.86±4.13	20.03±1.02	13.04±0.44
Random	20%-Mask	9.96±0.12	15.40±0.28	40.04±0.02	38.53±0.01	3.80±0.01	31.80±0.06	9.25±0.01	9.88±0.02	32.91±2.61	60.30±5.91	18.01±0.93	11.93±0.94
	40%-Mask	10.40±0.31	16.12±0.33	41.52±0.41	40.24±0.01	3.82±0.03	31.79±0.04	9.41±0.01	9.95±0.08	31.40±1.10	54.03±1.13	17.89±1.27	11.38±0.40
	60%-Mask	10.66±0.28	16.91±0.53	43.23±0.55	41.23±0.01	3.80±0.04	31.76±0.05	9.31±0.15	9.88±0.09	34.34±2.71	61.96±9.15	18.84±1.25	12.44±0.98
	80%-Mask	11.13±0.14	17.67±0.19	43.96±0.01	43.05±0.55	3.78±0.01	31.72±0.03	9.23±0.01	9.84±0.02	34.68±2.80	64.10±8.08	19.05±0.96	12.57±1.02
No Masking		9.33±0.13	14.24±0.18	38.57±0.32	36.09±0.49	3.79±0.01	31.73±0.02	9.30±0.03	9.88±0.03	31.91±1.35	56.49±2.54	17.63±0.97	11.57±0.49

Table 9: Performance under missing values on 2-day scenario.

Datasets		AQI-19				Speed-19*				Intensity-22			
Masking Strategy		MAE	RMSE	MAPE(%)	MRE(%)	MAE	RMSE	MAPE(%)	MRE(%)	MAE	RMSE	MAPE(%)	MRE(%)
Zero	20%-Mask	10.48±0.21	15.73±0.23	44.37±1.28	40.54±0.82	3.84±0.01	31.86±0.05	9.35±0.04	9.99±0.04	50.06±6.65	89.00±13.90	26.06±2.03	18.12±2.40
	40%-Mask	11.05±0.07	16.78±0.13	44.64±1.19	42.76±0.28	3.82±0.03	31.85±0.05	9.33±0.06	9.95±0.08	53.31±0.02	94.52±0.57	29.38±0.70	19.29±0.01
	60%-Mask	11.22±0.45	17.21±0.75	46.81±1.28	43.42±1.72	3.83±0.02	31.84±0.04	9.38±0.08	9.97±0.06	54.33±7.93	96.30±14.73	28.86±3.89	19.66±2.87
	80%-Mask	12.28±0.00	19.05±0.00	51.12±0.00	47.52±0.00	3.82±0.02	31.83±0.05	9.41±0.10	9.94±0.06	56.17±5.74	99.93±10.67	29.99±3.51	20.33±2.07
Random	20%-Mask	10.44±0.09	15.93±0.04	43.41±1.98	40.41±0.34	3.83±0.00	31.87±0.07	9.32±0.05	9.96±0.02	51.75±7.53	92.27±15.45	26.69±2.90	18.73±2.73
	40%-Mask	10.96±0.12	16.74±0.27	45.10±1.23	42.43±0.47	3.83±0.02	31.85±0.04	9.42±0.08	9.97±0.06	50.93±9.79	89.54±18.50	26.92±5.07	18.44±3.54
	60%-Mask	11.06±0.08	16.95±0.24	45.94±1.28	42.81±0.32	3.82±0.02	31.84±0.04	9.37±0.07	9.96±0.05	51.76±4.47	92.00±10.11	27.44±2.26	18.73±1.62
	80%-Mask	12.28±0.00	19.05±0.00	51.12±0.00	47.52±0.00	3.82±0.01	31.82±0.06	9.32±0.04	9.94±0.03	53.20±6.37	94.41±14.30	28.13±2.32	19.26±2.30
No Masking		10.04±0.19	15.12±0.26	42.62±0.52	38.84±0.75	3.80±0.01	31.78±0.02	9.32±0.03	9.89±0.03	50.59±0.04	89.10±7.36	26.68±1.69	18.31±1.14

Table 11: Ablation study from the data perspective on AQI-19 for 3-day forecasting, where P, F, and D represent Past, Future, and Data exogenous variables respectively.

P	F	U	MAE	RMSE	MAPE (%)	MRE (%)
✓	-	-	14.26±0.78	21.13±0.77	71.30±6.43	55.23±3.02
-	✓	-	10.94±0.28	16.25±0.38	46.23±1.60	42.38±1.08
-	-	✓	14.55±0.63	21.42±0.60	70.16±9.39	56.33±2.44
✓	-	✓	14.20±0.10	20.83±0.35	69.91±0.12	55.02±0.38
-	✓	✓	10.54±0.10	15.83±0.12	44.59±0.19	40.84±0.39
✓	✓	-	10.49±0.28	15.85±0.47	43.71±0.70	40.62±1.08
✓	✓	✓	10.41±0.12	15.51±0.16	44.65±0.08	40.34±0.47

**Figure 8: Ablation study on AQI-19 comparing ExoST, w/ Selector, and w/ Balancer variants in 2-day forecasting horizons.****Figure 9: Ablation study on AQI-19 comparing ExoST, w/ Selector, and w/ Balancer variants in 3-day forecasting horizons.****Table 10: Ablation study from the data perspective on AQI-19 for 2-day forecasting, where P, F, and D represent Past, Future, and Data exogenous variables respectively.**

P	F	D	MAE	RMSE	MAPE (%)	MRE (%)
✓	-	-	14.71±0.98	21.53±0.82	74.15±8.44	56.91±3.79
-	✓	-	10.71±0.40	16.05±0.55	45.33±2.40	41.44±1.54
-	-	✓	14.42±0.81	21.34±1.01	69.23±8.53	55.81±3.10
✓	-	✓	14.35±0.24	21.24±0.52	71.57±1.48	55.52±0.92
-	✓	✓	10.32±0.02	15.61±0.02	43.22±0.13	39.93±0.08
✓	✓	-	10.27±0.33	15.67±0.57	42.59±0.92	39.73±1.27
✓	✓	✓	10.04±0.19	15.12±0.26	42.62±0.52	38.84±0.75

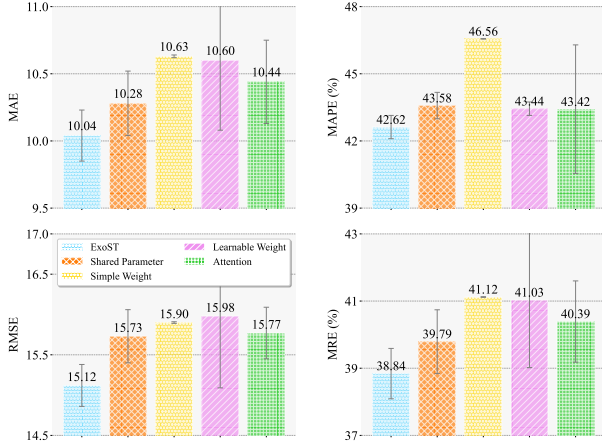


Figure 10: Different strategy performance comparison on AQI-19 dataset comparing share parameter, simple weight, learned parameter and attention variants on 2-day scenario.

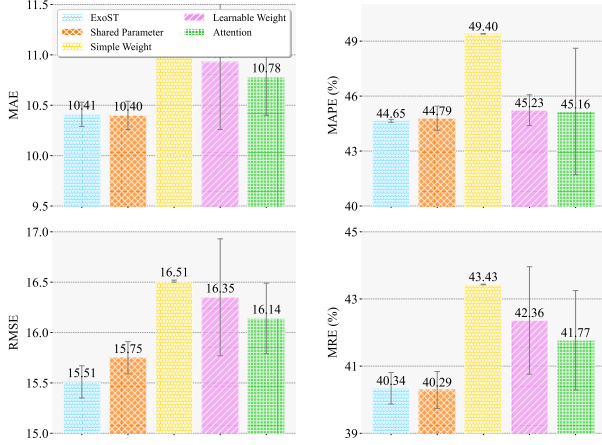


Figure 11: Different strategy performance comparison on AQI-19 dataset comparing share parameter, simple weight, learned parameter and attention variants on 3-day scenario.

B.3.2 Strategy Study. We first formalize the four strategies in detail through formulas:

- **Sharing Parameter:** A single spatio-temporal encoder is re-used for both exogenous streams:

$$Y^p = \phi_{st}^{\text{shared}}(X^{p'}), \quad Y^f = \phi_{st}^{\text{shared}}(X^{f'})$$

The forecast is obtained by averaging the two outputs:

$$\hat{Y} = \frac{1}{2} Y^p + \frac{1}{2} Y^f.$$

- **Simple Weight:** Each stream is processed by its own encoder 3.2. The final prediction employs fixed, equal weights:

$$\hat{Y} = \frac{1}{2} Y^p + \frac{1}{2} Y^f.$$

- **Learnable Weight:** Let $w_{\text{init}} \in \mathbb{R}^2$ be a learnable vector, normalized by softmax:

$$w = \text{Softmax}(w_{\text{init}}), \quad w_0 + w_1 = 1.$$

Given the two outputs of the backbone, the fusion is

$$\hat{Y} = w_0 Y^p + w_1 Y^f + (Y^p + Y^f),$$

where the last term is a residual connection.

- **Attention:** Let Y^p, Y^f denote the intermediate hidden states produced by the two branches before the final read-out layer. For each directional attention we use shared projection matrices $W_q, W_k, W_v \in \mathbb{R}^{H \times H}$.

Future \rightarrow Past.

$$Q^f = Y^f W_q, \quad K^p = Y^p W_k, \quad V^p = Y^p W_v,$$

$$\alpha_{f \rightarrow p} = \text{softmax} \left(\frac{\sum_{h=1}^H (Q_{:,t,h}^f \cdot K_{:,t,h}^p)}{\sqrt{H}} \right),$$

$$A_{f \rightarrow p} = \alpha_{f \rightarrow p} \odot V^p,$$

$$Y_{\text{enh}}^p = Y^p + A_{f \rightarrow p}.$$

Past \rightarrow Future.

$$Q^p = Y^p W_q, \quad K^f = Y^f W_k, \quad V^f = Y^f W_v,$$

$$\alpha_{p \rightarrow f} = \text{softmax} \left(\frac{\sum_{h=1}^H (Q_{:,t,h}^p \cdot K_{:,t,h}^f)}{\sqrt{H}} \right),$$

$$A_{p \rightarrow f} = \alpha_{p \rightarrow f} \odot V^f,$$

$$Y_{\text{enh}}^f = Y^f + A_{p \rightarrow f}.$$

Final Prediction.

$$\hat{Y} = \frac{1}{2} Y_{\text{enh}}^p + \frac{1}{2} Y_{\text{enh}}^f,$$

As Figures 10 and 11 show, we can observe that: ❶ In the 2-day horizon, **ExoST** maintains its advantage, while *Simple Weight* and *Learnable Weight* exhibit amplified weaknesses: the former's static weighting fails to handle increased uncertainty in longer forecasts, and the latter, despite its adaptable weights, amplifies noise from future exogenous signals due to lacking day-to-day context modeling. ❷ Although all methods show increasing errors across horizons of 1-day to 3-day, **ExoST** consistently suppresses error accumulation better than alternatives.

C MORE DISCUSSION

C.1 Limitation

In this paper, we propose a new framework for modeling exogenous variables in spatio-temporal forecasting: **ExoST**. This “select, then balance” design addresses the inconsistent effects of variables and the imbalanced effects of types. Extensive experiments demonstrate the superiority of our method in terms of effectiveness, universality, and robustness. Although we have made some attempts in this direction, there are still some limitations that need to be addressed:

- First, our method assumes that spatio-temporal exogenous variables are available in real-time and are synchronized with the target system. In reality, it may not be possible to acquire real-time exogenous information at all times. Even when available, differing equipment may lead to inconsistent and mismatched sampling rates. While we conducted preliminary experiments using random masking to simulate asynchronous and non-real-time data, and our model showed some robustness, a deeper investigation into this issue is left for future work.
- Second, our model currently assumes that spatio-temporal exogenous variables are numerical sensor signals. However, real-world scenarios often involve diverse, heterogeneous exogenous information, such as language and visual information. Recent research has explored using Large Language Models (LLMs) for time series [1, 11, 24, 35, 41, 49] and spatio-temporal forecasting [31, 34, 36, 58], hoping that LLMs can gain numerical prediction capabilities through various alignment techniques. However, some studies have raised significant doubts about these approaches [50]. Different from these views, we

believe that language can be more effectively viewed as sparse, discrete exogenous auxiliary information. The key challenge lies in how to leverage this information to enhance various spatio-temporal tasks.

C.2 Future Direction

Based on these analyses, we identify two key areas for future work:

- For spatio-temporal forecasting tasks, we believe the core challenge is to use the semantic representations of exogenous variables to provide an auxiliary spatio-temporal backbone network with interventional information, allowing it to respond to dynamic changes. This approach is distinct from using language models as the primary prediction backbone.
- For spatio-temporal reasoning tasks, we believe the core essence is to activate the intrinsic capabilities of language models to analyze the underlying causes of spatio-temporal changes and provide logical knowledge-based answers.